



HAZRUNOFF
PROJECT

“Integration of sensing and modelling technologies for early detection and follow-up of hazmat and flood hazards in transitional and coastal waters”

D1.1 Using remote sensing products and services for early warning and model validation for hazards in transitional water



Funded by
European Union
Civil Protection
and Humanitarian Aid

WP	Remote sensing (for early warning and model validation)
Action	With the purpose of improving early detection, early warning, model initialization and model validation on flood and pollution hazards in transitional waters, the following parameters are selected to be studied: water level, turbidity, oil slick identification, and chemical spill detection.
last updated	06/12/19
version	V0.1
authors	C Boedinger, K Schenk (EOMAP)
participants	EOMAP

Disclaimer

"This document covers humanitarian aid activities implemented with the financial assistance of the European Union. The views expressed herein should not be taken, in any way, to reflect the official opinion of the European Union, and the European Commission is not responsible for any use that may be made of the information it contains."

CONTENTS

INTRODUCTION	4
SATELLITE SENSORS AND DATA.....	5
Sentinel-2.....	5
Landsat 8	6
Sentinel-1.....	7
SATELLITE DATA PROCESSING WORKFLOWS AND PRODUCTS	8
Turbidity.....	10
Water Coverage.....	13
Oil and Chemical Spill	14
PILOT CASES	26
Study Areas	26
Pilot Case Studies: Discussion of Results	29
QUALITY CONTROL.....	39
SETUP OF MONITORING SYSTEMS.....	41
Data Selection	41
Automated data access from archives.....	42
INTEGRATION IN THE HAZRUNOFF WEBTOOL.....	42
Automated product upload using Geoserver API	43
Visualization in the HazRunOff Webtool.....	44
MODEL VALIDATION FOR HAZARDS IN TRANSITIONAL WATER	45
CONCLUSIONS AND RECOMMENDATIONS.....	46
APPENDIX.....	47
Spill Occurrences provided by PHE.....	47

Introduction

This report was prepared by EOMAP as part of work package 1 (WP1), Detecting, sensing and sampling. The scope of D1.1 was to support civil protection services, water pollution response services, coastal modellers and entities working on remote sensing with their activities in hazard early detection, early warning, model initialization and model validation on flood and pollution hazards in transitional waters.

For this purpose, EOMAP has implemented operational monitoring services in four pilot sites using free & open satellite imagery from various sensors. Satellite data archives are automatically searched and pre-defined criteria (e.g. maximum cloud coverage thresholds) fulfilling data is downloaded. Data from both optical and radar sensors are analysed and processed by EOMAP's Modular Inversion and Processing System (MIP). The results are pushed and stored on an online server and seamlessly ingested into the HazRunOff platform developed as part of WP3 (Figure 1).

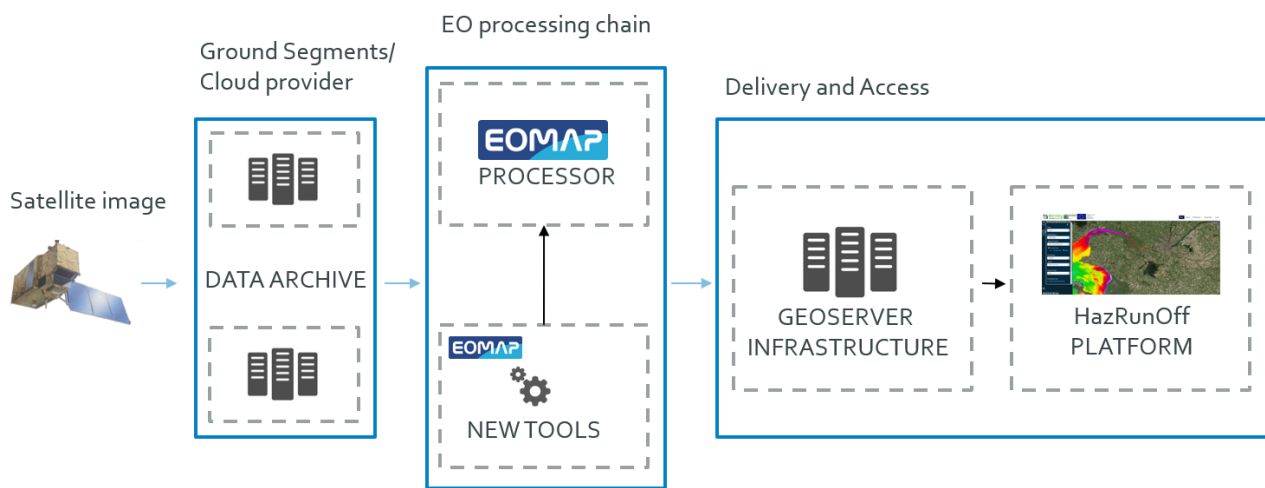


Figure 1: EOMAPs workflow from the space to the ground segment and the user.

Remotely sensed imagery can serve stakeholders through timely, area-wide provision of relevant environmental data. The number of satellite missions is rapidly increasing throughout the last decades. In addition to the already operating sensors, several continuing and new missions have already been announced. This allows for increasingly dense time series and repeated imaging, which is crucial for rapid emergency detection and response. To minimize the time in between image acquisition, processing and provision to the end user, special demands are questioned from the processing chain. A

high degree of automatization is mandatory as interactions during processing are depending on the availability of personal and consume both time and resources.

In the following, the conceptual design, setup and results of operational workflows for turbidity, water coverage and oil spill as well as the experimental detection of chemical spills are described. Furthermore, the integration of the data into the HazRunOff webtool, the seamless ingestion into the modelling part of the project and the provision to the user are explained. This work is part of the project activity 1.1 Remote sensing (for early warning and model validation).

Satellite Sensors and Data

In this study we have used optical satellite data from European Space Agency's (ESA) Sentinel-1 and Sentinel-2 sensors as well as U.S. Geological Survey's (USGS) Landsat 8. Those satellites have a free & open data policy, the needed high spatial resolution for river and estuary monitoring and a near global coverage.

SENTINEL-2

Sentinel-2 has three bands (band 2, 3 and 4, see Figure 2) in the visible spectral range which are recorded in a spatial resolution of 10m, and a further 10m spatial resolution spectral band in the near infrared region (NIR). The other spectral bands are of coarser resolution and are used for the atmospheric correction, adjacency correction and removal of sun glint effects (see next section on Landsat 8). There are currently two Sentinel-2 satellites in space, Sentinel-2A and Sentinel-2B with two more to come. Revisit time for both satellites is 5 days at the equator and 2-3-days at mid-latitude.

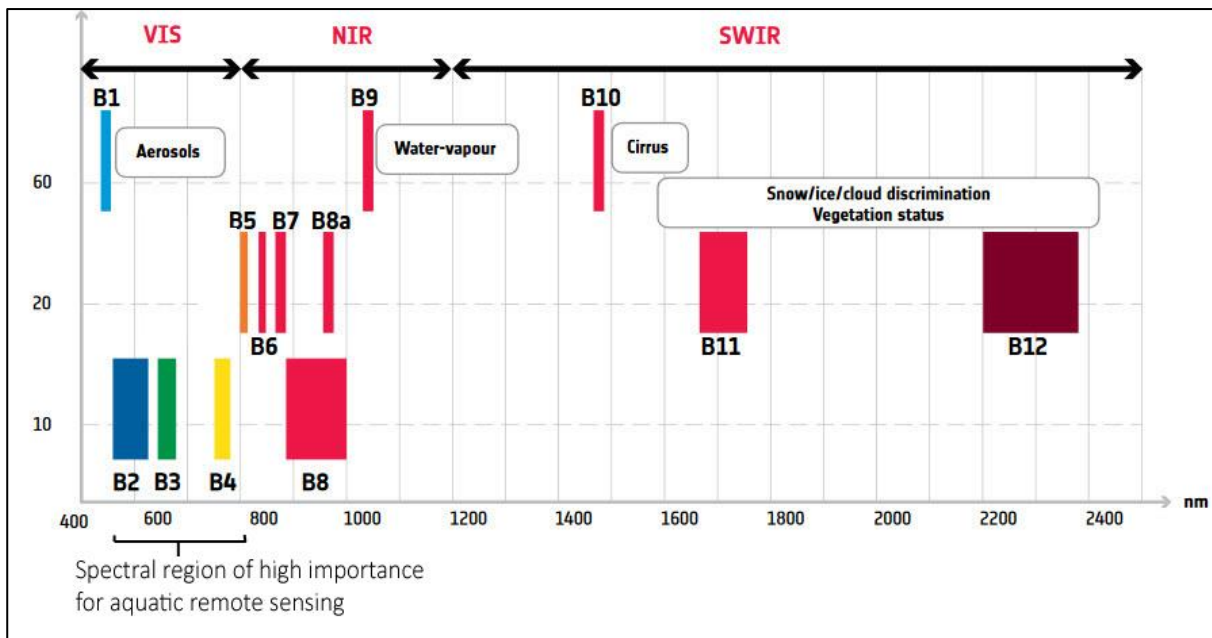


Figure 2: Spectral bands of the Sentinel-2a and b sensors. Three spectral bands are of particular importance for aquatic remote sensing (source: Modified from ESA, 2019)

Note, that all used satellite raw data can be accessed through the European Space Agency's archive. The most comfortable access to the data is through the Sentinel-HUB EoBrowser online portal¹.

LANDSAT 8

Landsat 8 has 11 spectral bands in total, 3 bands in the visible range and 3 more bands in the infrared region with 30m spatial resolution. Like Sentinel-2, the other bands are coarser and/or used for pre-processing. The satellite features two sensors of which OLI includes the visible, NIR and SWIR bands. The TIRS sensor features the thermal infrared (TIR) bands with a rather coarse spatial resolution of 100m (Figure 3). Landsat 8 has been launched in 2013 and a new satellite of the continuation mission is scheduled to launch by the end of 2020. Revisit rate at mid-latitude is 16 days.

¹ <https://apps.sentinel-hub.com/eo-browser/>

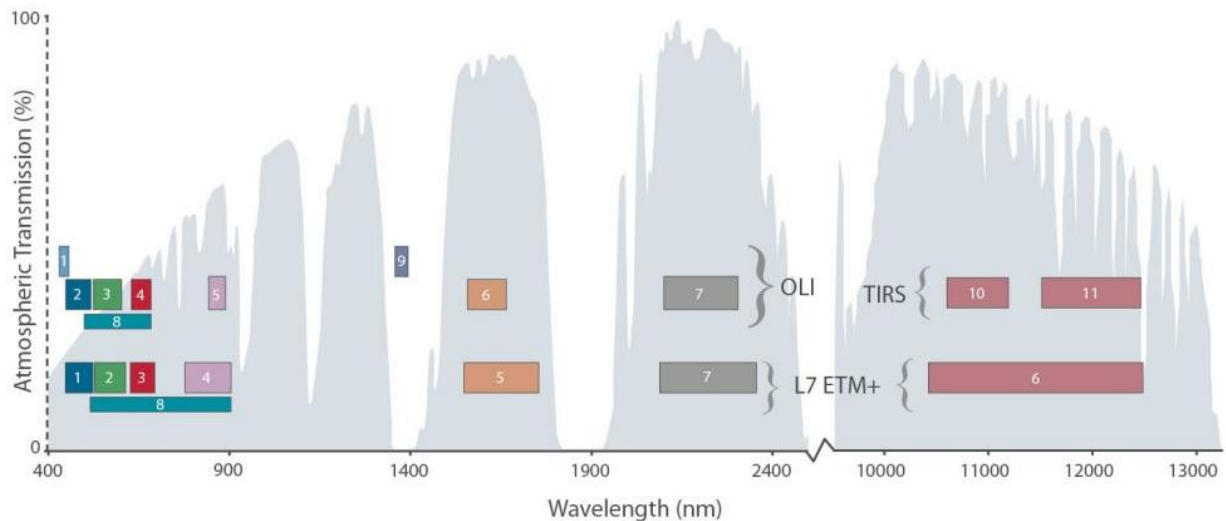


Figure 3: Spectral bands of the Landsat 8 and Landsat 7 (not used in HazRunOff) sensors and the wavelength dependency of atmospheric transmission (source: NASA, 2019).

SENTINEL-1

Like the other Sentinels, Sentinel-1 is part of ESA's Copernicus program but differs from the other sensors used in the project as it is an active radar sensor. Sentinel-1 is a C-Band synthetic aperture radar (SAR) satellite, which acquires images at two polarizations (VV+VH). The radar system is able to collect images at different spatial resolutions, most commonly in interferometric wide-swath (IW) with 10m spatial resolution of the ground range detected (GRD) product (Figure 4). The swath width of Sentinel-1 in IW mode is 250km meaning that images are collected in 250km long stripes. With further distance from the sensor the incidence angle of the acquisition increases. This results in distortions which need to be corrected. ESA provides data with these corrections applied in form of the GRD products. The Sentinel-1 constellation includes two satellites Sentinel-1A and Sentinel-1B, with at least two more satellites to

come. The revisits time and spatial coverage of the IW SAR system is higher than that of the optical sensors presented before. Data at mid-latitude is collected every 2 days.

Satellite Data Processing Workflows and Products

For the retrieval of satellite-derived water quality data, the physics-based Modular Inversion and Processing System (MIP), developed by EOMAP, has been applied to the

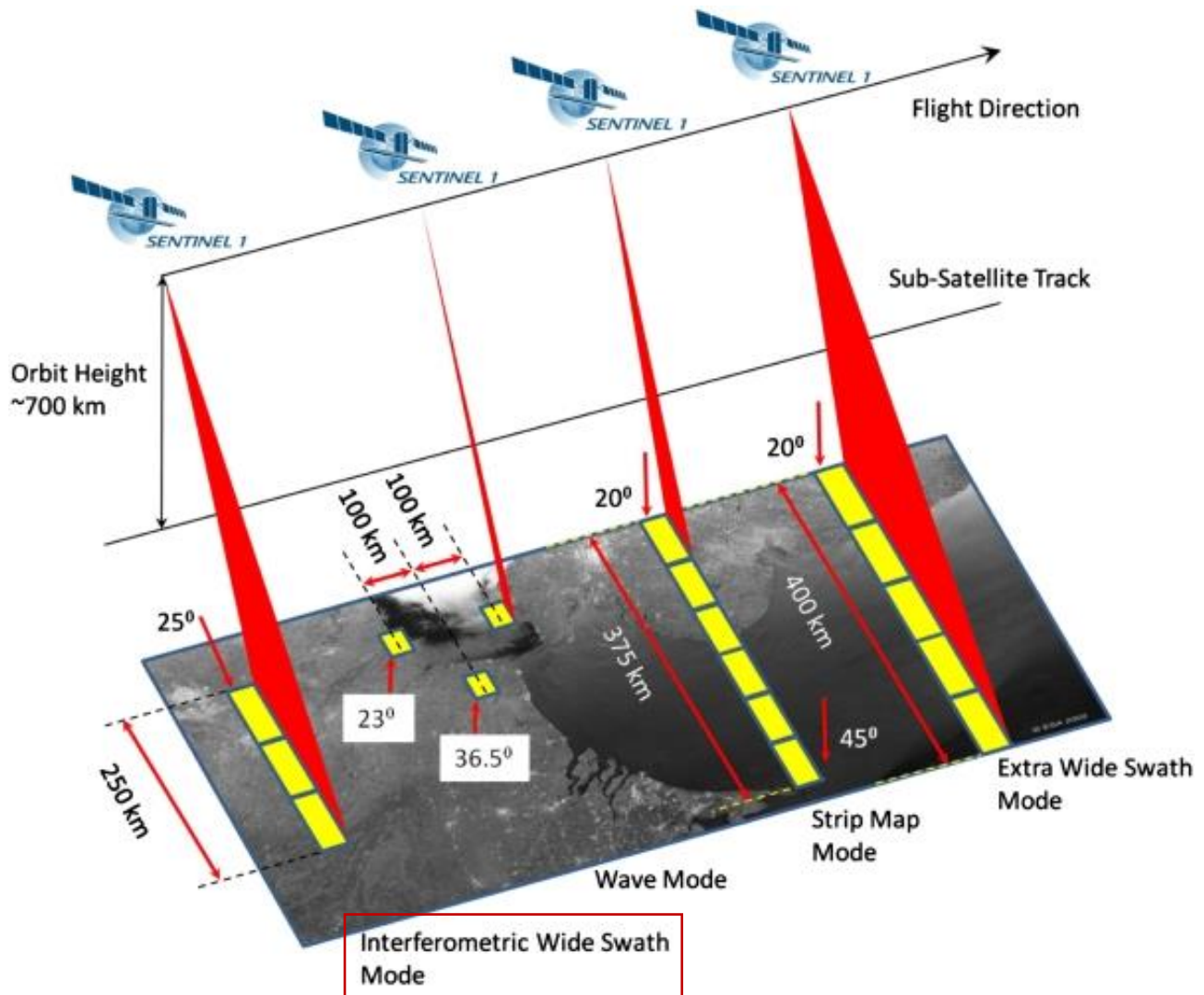


Figure 4: Sentinel-1 acquisition modes. Data collected with the "Interferometric Wide Swath Mode" are used in this project (source : modified from ESA, 2019).

satellite imagery. This sensor-independent approach includes all the relevant processing steps to guarantee a robust, standardised and operational retrieval of water quality parameters from various satellite data sources. The advantage of physics-based methods is that they do not require a priori information about the study area and can therefore be applied independently of satellite type and study area.

MIP imbeds sensor-independent algorithms and processing modules to derive consistent water quality parameters for multiple scales through several different satellite sensors. The algorithms take all relevant environmental impacts into account and do so for each individual measurement and pixel according to the current state-of-the-art, including:

- a. water, land, cloud identification
- b. estimation and correction of atmosphere and aerosol impacts^{2 3}
- c. correction of altitude level impacts⁴
- d. correction of adjacency impact (light scattering into the water signal from adjacent land surfaces)⁵
- e. correction⁶ or flagging⁷ of sun glint impact
- f. retrieval of in-water absorption and scattering as physical measures⁸
- g. accounting for varying spectral slopes of specific inherent optical properties⁹
- h. provision of uncertainty measures and flagging procedures
- i. accounting for the full bidirectional effects in the atmosphere, at the water-atmosphere boundary layers and in-water, using a fully coupled radiative transfer model
- j. application of procedures to minimize errors, resulting from the coupled interaction of light between atmosphere, water surface and in-water on the signal, through coupled inversion procedures

The different workflow steps from satellite raw imagery import to value-added water quality retrieval are displayed in Figure 5.

² Heege, T., Kiselev, V., Wettle, M., Hung N.N. (2014): Operational multi-sensor monitoring of turbidity for the entire Mekong Delta . Int. J. Remote Sensing, Special Issues Remote Sensing of the Mekong, Vol. 35 (8), pp. 2910-2926

³ Richter, R., Heege, T., Kiselev, V., Schläpfer, D. (2014): Correction of ozone influence on TOA radiance. Int. J. of Remote Sensing. Vol. 35(23), pp. 8044-8056, doi: 10.1080/01431161.2014.978041

⁴ Heege, T., Fischer, J. (2004): Mapping of water constituents in Lake Constance using multispectral airborne scanner data and a physically based processing scheme. Can. J. Remote Sensing, Vol. 30, No. 1, pp. 77-86

⁵ Kiselev, V., Bulgarelli, B. and Heege, T., (2015). Sensor independent adjacency correction algorithm for coastal and inland water systems. Remote Sensing of Environment, 157: 85-95, ISSN 0034-4257, <http://dx.doi.org/10.1016/j.rse.2014.07.025>

⁶ Heege, T. & Fischer, J. (2000): Sun glitter correction in remote sensing imaging spectrometry. SPIE Ocean Optics XV Conference, Monaco, Oct. 16-20.

⁷ EU FP7-Projekt GLASS: WP4 Validation report (29.2.2016): www.glass-project.eu/assets/Deliverables/GLaSS-D4.2.pdf

⁸ Bumberger J., Heege T., Klinger P., et al. (2017): Towards a Harmonized Validation Procedure for Inland Water Optical Remote Sensing Data using Inherent Optical Properties, Rem. Sens. 2017(9), 21p.

⁹ Heege T., Schenk K., Klinger P., Broszeit A., Wenzel J., Kiselev V. (2015): Monitoring status and trends of water quality in inland waters using earth observation technologies. Proceedings "Water Quality in Europe: Challenges and Best Practice" UNESCO-IHP European Regional Consultation Workshop, Koblenz, Germany, Dec 2015, p. 1-4

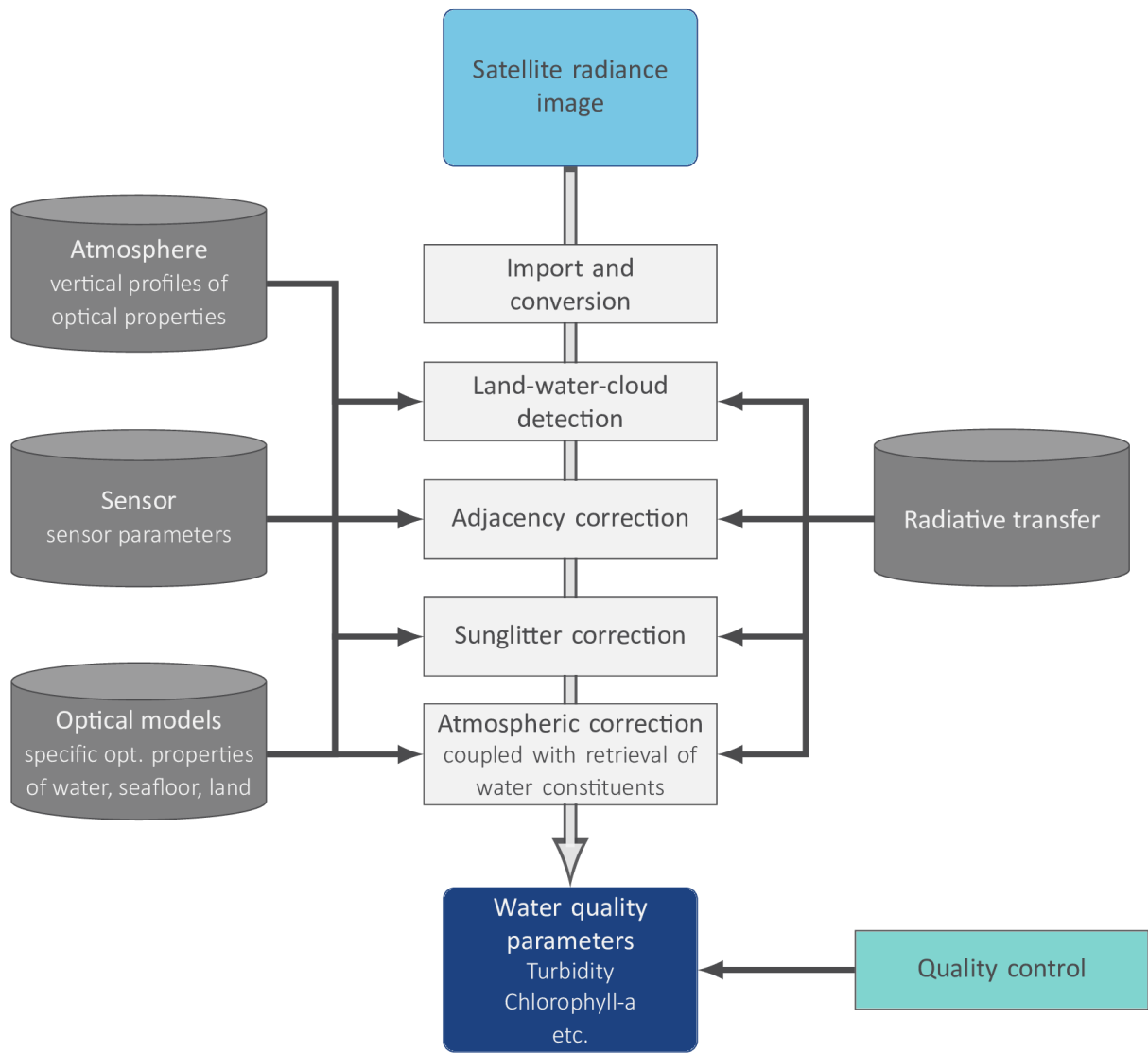


Figure 5: EOMAP's physics-based workflow to derive satellite-based water quality and water depth

MIP is the most established, sensor-independent and operational aquatic remote sensing processing system for the full range of high, medium and low-resolution satellite sensors. Fully-automated water monitoring processors are installed in satellite ground segments worldwide (Europe, Australia, Asia and America), to ensure fast and efficient access to a wide range of satellite data. The data processing and orchestration software, the EOMAP Workflow System (EWS) allows for continuous, daily production.

The following products have been delivered:

TURBIDITY

Turbidity (TUR) is a key parameter of water quality and is linearly related to the backward scattering of light due to organic and inorganic particles in water. Turbidity is furthermore linearly related to Total Suspended Matter (TSM) at low to moderate turbidity values. High concentrations of particulate matter affect light penetration and productivity, recreational values, and habitat quality, and cause lakes to fill in faster. In streams, increased sedimentation and siltation can occur, which can result in harm to habitat areas for fish and other aquatic life. Particles also provide attachment places for other pollutants, notably metals and bacteria. For this reason, turbidity can be used as an indicator of potential pollution in a water body. Excessive turbidity, or cloudiness, in drinking water is aesthetically unappealing, and may also represent a health concern. Turbidity can provide food and shelter for pathogens. If not removed, turbidity can promote regrowth of pathogens in the distribution system, leading to waterborne disease outbreaks, which have caused significant cases of gastroenteritis throughout the world. Although turbidity is not a direct indicator of health risk, numerous studies show a strong relationship between removal of turbidity and removal of protozoa. The particles of turbidity provide "shelter" for microbes by reducing their exposure to attack by disinfectants. Microbial attachment to particulate material has been considered to aid in microbe survival. Fortunately, traditional water treatment processes can effectively remove turbidity when operated properly¹⁰.

¹⁰Swanson, H.A., and Baldwin, H.L.(1965) : A Primer on Water Quality. U.S. Geological Survey.

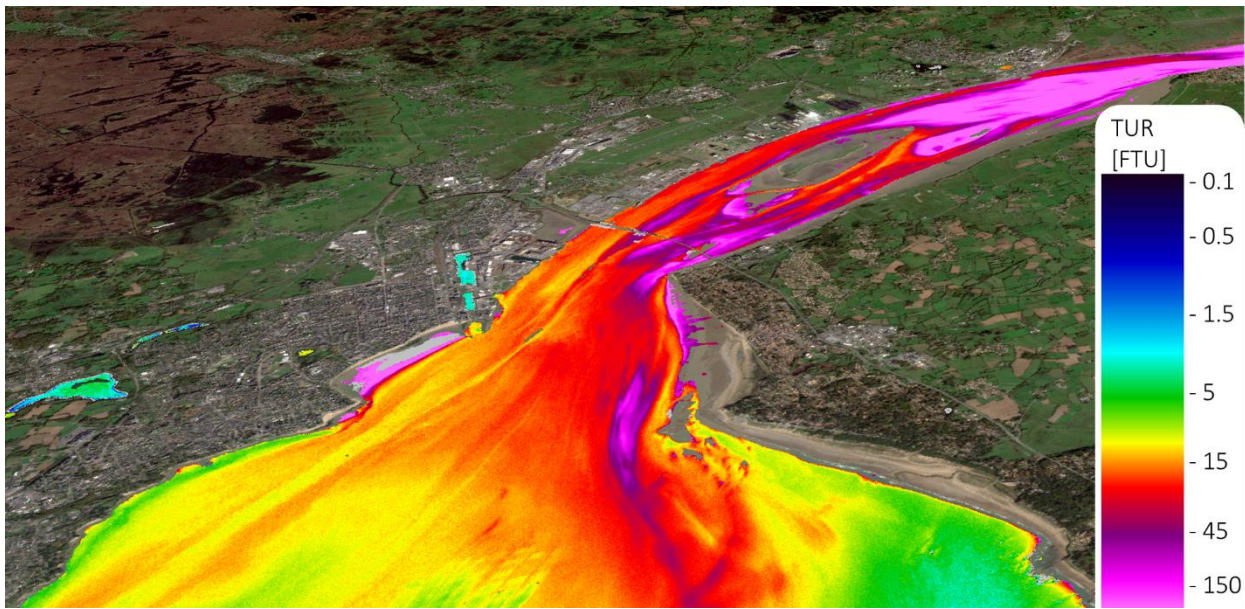


Figure 6: Turbidity in the Loire estuary and the EOMAP colorscale.

The measurement unit is Formazine Turbidity Unit (FTU). Satellite derived turbidity is determined by the backward scattering of light between 450 to 800nm, physically retrieved using satellite data. The geometrical properties of the in-situ measurement device and wavelength used may differ in comparison to the satellite product. For example, the standard FTU determination, a measure of turbidity similar to the Nephelometric Turbidity Unit (NTU), is based on the measurement of light scattered within a 90° angle from a beam directed at the water sample. Alongside temporal differences in satellite and in-situ measurements, different sampling depths and the measurement location, this needs to be considered when comparing and interpreting satellite derived vs. in-situ measured turbidity values. Standard relation of EOMAP concentrations to inherent optical properties are defined as 1 FTU = 0.619 1/m total scattering at 550nm, 1 FTU = 0.0118 1/m backward scattering at 550nm and a ratio $bb/b = 0.019$. Note that there is no physical way to discriminate optically shallow water with visible ground and turbidity. For this reason, turbidity measures make sense only over optically deep waters. Shallow water areas are not statically masked in this project as the focus is on flood monitoring inside transitional waters with strong tidal variation. An example for the satellite-based turbidity product is given in Figure 6.

WATER COVERAGE

Water extent (WEX) product discriminates between land/clouds and water pixels based on typical reflectance and backscatter features in visible, near/shortwave infrared region and different radar polarizations. Data on water extent is the basis of flood/inundation modelling and identification of areas at risk. WEX can serve both the entities concerned with modelling for ex ante validation of the flood models and predictions as well as authorities seeking to get an overview on areas affected by current or past flooding.

Water coverage is derived from both optical and radar data. In case of optical imagery, the underlying algorithms take advantage of the strong differentiation of land/water in the infrared region. Water reflectance is usually low and declining towards longer wavelengths starting from the near infrared region. Strong load with sediments may hamper the discrimination as the light is reflected from suspended particles.

The water coverage products profits from the capability of the Sentinel-1 SAR system to penetrate clouds. Data can also be collected during weather conditions typical for flooding events. The water detection using SAR imagery is based on the different backscatter behaviour of the radar. Over calm water the incoming signal is almost completely reflected away from the sensor while on land more radiation is reflected back towards the sensor. Wind and very shallow water alter the backscattering properties. Pre-processing and postprocessing steps need to account for these as well as for the radar inherent noise called *speckle*. An example from of Sentinel-1 raw data and its derivative water extent map is displayed in Figure 7.

These datasets are combined with digital elevation data from the Shuttle Radar Topography Mission (SRTM) to calibrate the retrieval and for an additional quality control.

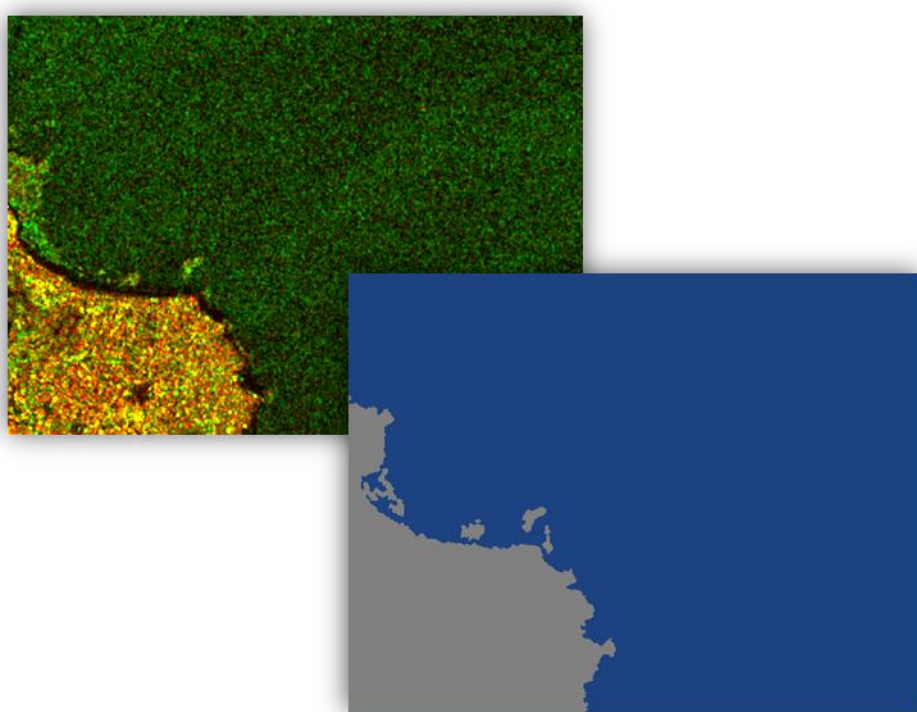


Figure 7: Pseudo-RGB from raw Sentinel-1 imagery. Derived binary water mask (blue is water).

OIL AND CHEMICAL SPILL

Coastal agencies and early responders require timely and accurate detection of oil and other chemical slicks of which some do not pose a danger to the environment. False alarms are a pending issue and consume both an excessive amount of time and money inside the responding entity. In case of a detection, the responder is asked to carry out expensive field campaigns to determine the chemical spilled. This is often done by helicopter and requires subsequent laboratory analysis. Therefore, false alarms either raised by to an actually wrong detection and false alarms due to a harmless chemical being spilled (legal spill) need to be reduced as much as possible. These demands are made of any oil spill warning system in place. Existing detection systems such as EMSA's CLEANSEANET¹¹ focus on SAR imagery. Detection of oil spills using SAR imagery relies on the dampening effect of oil on the water effect, thus reducing the backscatter. These areas appear dark in the images and further techniques such as object-based segmentation based on textural measures can be applied to separate them from the

¹¹ <http://www.emsa.europa.eu/csn-menu.html>

background¹². However, oil slicks are not the only phenomena that dampen the backscatter. Also, areas with low wind speed, wave shadows behind land or structures, shallow seaweed beds that calm the water just above them, glacial flour, biogenic oils, and whale and fish sperm have the same effect. Wind speed poses a further limitation to the detectability as at minimum 1.5 m/s are required and above a maximum wind speed of 6–10 m/s will again remove the characteristic effects of the oil on water. The most accepted limits are 1.5 m/s to 10 m/s. This limits the environmental window of application of both radar and optical imagery for detecting oil slicks.

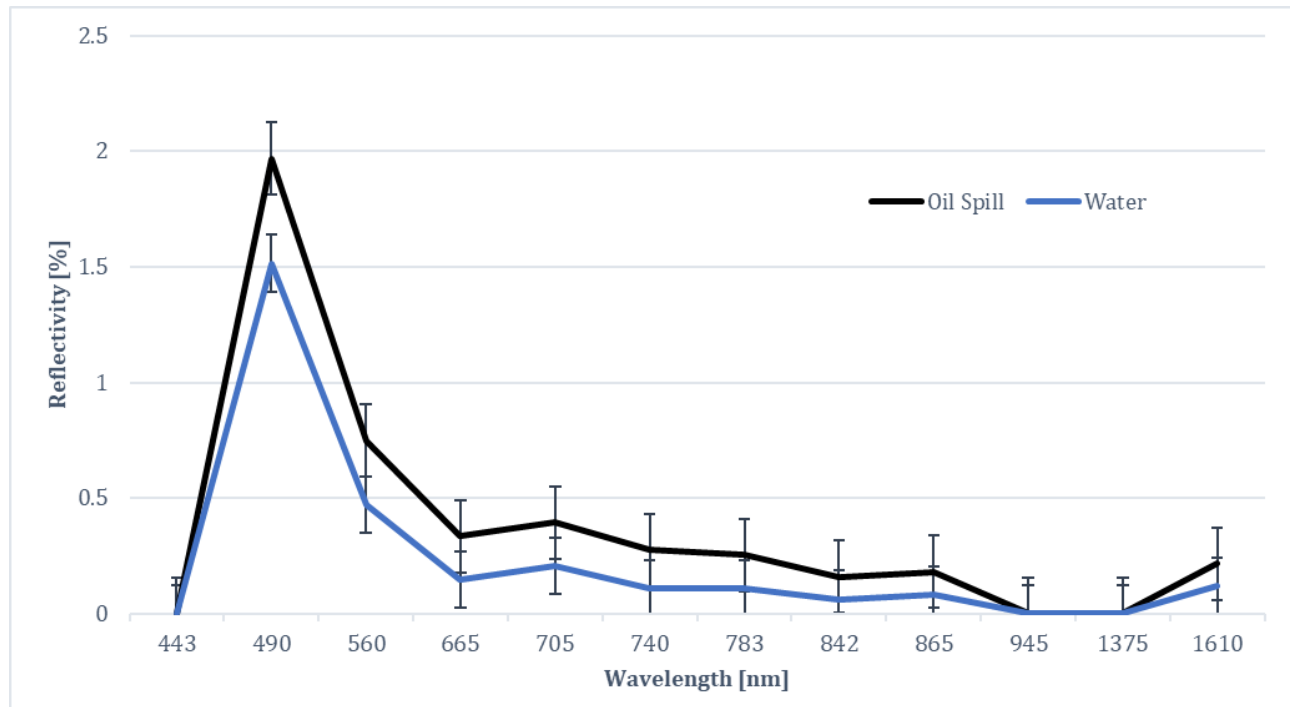


Figure 8: Comparison between water surface reflectivity of water and a slightly weathered oil spill. Error bars show the variation of the reflection values.

Optical imagery enhances the information space of the dual-polarization SAR data with the information of the visible and infrared region. The reflection at water surface of a weathered oil spill is slightly increased in the visible light region (Figure 8). Between 500 and 600nm and the NIR/SWIR region the differences are weaker. In thermal infrared the characteristically higher brightness temperature of oil can be used as an

¹² Skrunes, S., Brekke, C., Eltoft, T. (2014): Characterization of Marine Surface Slicks by Radarsat-2 Multipolarization Features. IEEE TRANSACTIONS ON GEOSCIENCE AND REMOTE SENSING, VOL. 52, NO. 9, DOI: 10.1109/TGRS.2013.2287916.

indicator. Again, textural measures as well as band ratioing can be used in a segmentation and classification environment. Depending of course on local weather conditions and the age of the spill, slicks often exhibit elongated shapes. With more time passing by since the spill event, the slick becomes increasingly less coherent through wind, weathering and wave motion. Object-based classification approaches therefore often come to a limit when confronted with heterogenous spills and manual correction and inspection is inevitable.

Although direct comparison between optical and radar imagery is practically impossible due to the offset in imaging time between both sensors, the spill probability can be increased if two images with a sufficiently small-time gap are compared with each other. Therefore, both images are classified, inspected separately and cross-checked with each other. If under consideration of the expected ocean movement a spill can be identified within both images, the presence becomes more likely. The maximum time difference between both images that still allows for a valid comparison, depends again on the local environmental conditions and the magnitude of the spill as well as the solubility and weathering speed of the spilled material. Obviously, this approach is limited in an emergency response environment due to the dependency on at least two images being acquired and processed. However, if images with short temporal offset are given, the comparison can put further reliability to a spill detection system by decreasing the number of false alarms through independently analysing two vastly different satellite sensors.

WORKFLOW DESIGN

Oil and chemical spill detection services can be requested via the EOMAP contact details on the HazRunOff website or the EOMAP webpage as manual operator interaction is necessary during the processing chain. The operational services are not limited to the pilot case studies and can be requested globally.

An object-based process for SAR-based oil spill detection typically consists of three steps: image segmentation for dark-spot identification, feature extraction, and oil spill and look-alike discrimination. The spill detection workflow presented in this chapter is more holistic starting from data search, pre-processing to material discrimination and

reporting to the user (Figure 9). It is designed in a way that reduces operator interaction to a minimum and can be applied in an operational framework. It includes the processing chain for optical imagery from Sentinel-2. After automated checks for new scenes, the wind speed at the time of imaging is determined using NASA's EarthData API¹³. If the wind speed exceeds pre-defined ranges (1.5 m/s to 10 m/s for SAR imagery and 1.5 m/s to 12 m/s for optical imagery), the scenes are not downloaded or processed and a message is triggered informing the operator of unsuitable wind conditions and the affected image and sensor. In case the wind speed is within the pre-defined range, automated downloads are performed by the system and the processing chain starts as soon as the download is finished.

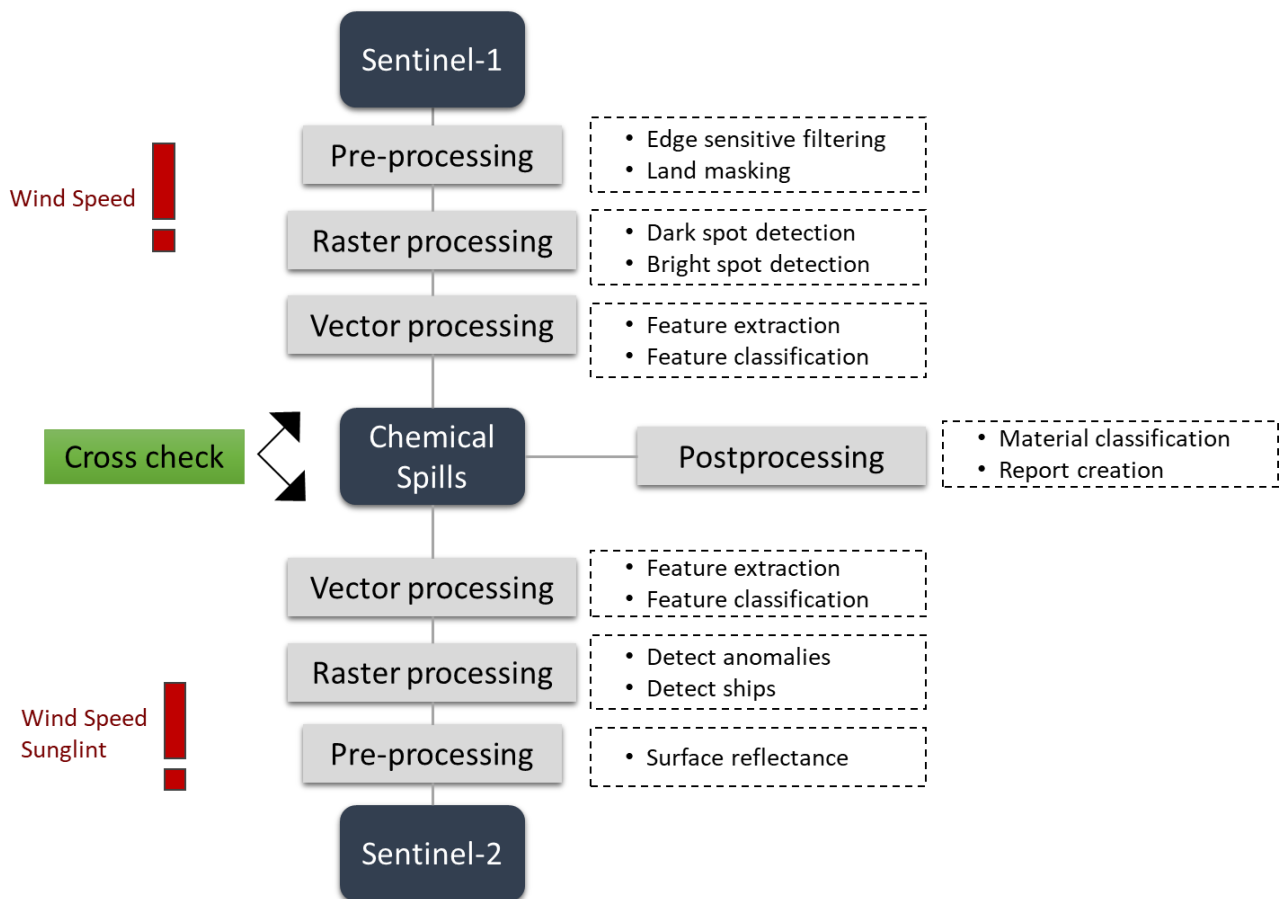


Figure 9: Workflow of an operational spill detection and classification system taking advantage of both optical and radar data.

¹³ <https://urs.earthdata.nasa.gov>

Pre-processing is a fundamental step that has significant impact on the detection rate. As an initial step, the land areas are masked, and the image is clipped to the region of interest. This reduces the time taken for processing in all subsequent steps, which is important for the fast delivery that is required in an emergency response framework. Sentinel-1 data are provided by ESA in an uncalibrated format that does not allow for comparison with pre-defined thresholds and other scenes. Therefore, the backscattering coefficient σ^0 (spoken sigma nought) has to be derived from the source data using supplied look-up tables for conversion and calibration. σ^0 is a normalised dimensionless number, comparing the strength observed to that expected from an area of one square metre. Due to the strong speckle noise in SAR imagery, pre-processing also includes filtering of the σ^0 product. While there are countless filtering techniques including some specifically designed for filtering of SAR data and removing speckle noise, we decided to use a bilinear filter. This filter has been adapted to preserve edges in the image and filter especially those areas, which do not exhibit edges and defined structures. By doing so the borders of the spills are preserved and the water areas as well as the spill itself are smoothed and more homogenous after filtering.

Using thresholding and object detection dark spots (spills) and bright spots (man-made objects e.g. ships) are identified within the image. These spots are isolated and vectorized as polygons. Several indices are calculated from the underlying raster data inside the polygonised features. These include Grey Level Co-Ocurrence Matrix (GLCM) texture measures in case of radar imagery as well as GLCM, band ratios and indices in case of optical imagery. An overview on parameters helpful in classifying spills and separating from look-alikes is given in Table 1.

Table 1: Raster and shape parameters used in a spill classification system. * = parameters derived for Sentinel-1 and Sentinel-2, ** =parameters derived for Sentinel-2 only. Shape features considering the underlying raster data or the neighbourhood in italic.

GLCM*	Band ratios (S-2 bands)**	Indices**	Shape features*
Contrast, Correlation Dissimilarity, Entropy, Mean, Variance	4/3, 4-3, 5/3, 2/11	NDVI, NDWI	Slick area, perimeter, complexity, <i>maximum contrast between object and background, distance to bright spot, number of neighbouring spots and number of spots in scene</i>

Of course, the parameters listed are not a complete list of all parameters available, but a condensed summary of features found useful for classification. Although classifiers such as Random Forest are well able to extract meaningful parameters from a set of predictors and assign to those a higher weighting during the classification, processing time increases with the number of variables used. As an example, Figure 10 shows a range of GLCM parameters calculated from Sentinel-1 VV polarized data. Energy and Homogeneity obviously work well in regions with thick and homogenous oil cover. However, contrast from the background is lost at the transition to water and less densely covered patches. These areas now appear dark and are especially difficult to distinguish further up in the scene. In contrast, Variance and Correlation prove to be more edge-sensitive increasing the separability of oil covered areas throughout the whole image.

Shape features are calculated based on the vectorized dark and bright spots. They can be distinguished into features calculated based on single features only and those that take the underlying raster data or the feature neighbourhood into account.

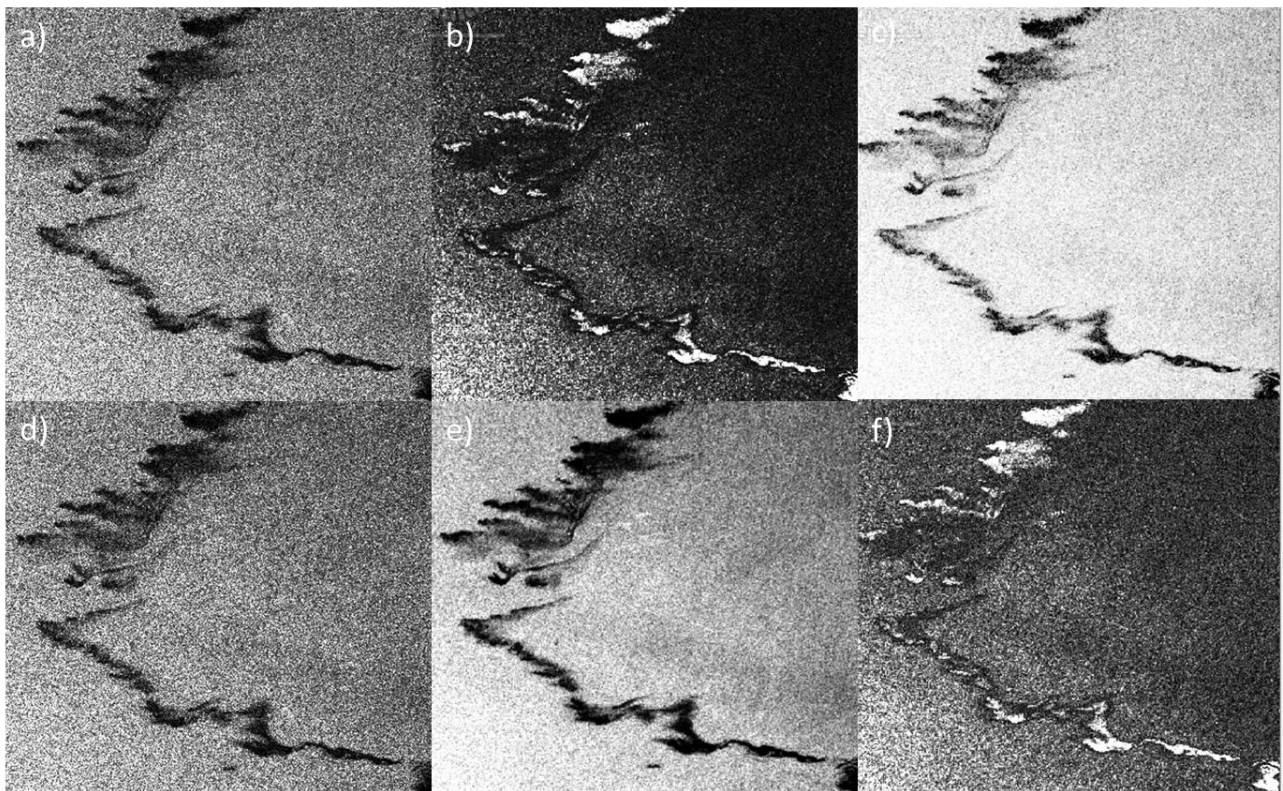


Figure 10: GLCM features calculated from Sentinel-1 SAR imagery (VV polarization). Example from the CLS Virginia collision north of Cape Corse in October 2018. a) sigma nought VV polarization b) GLCM Energy c) GLCM correlation d) GLCM mean e) GLCM variance f) GLCM homogeneity.

A similar concept is applied to the Sentinel-2. Differing from radar imagery, in the case of optical imagery also sun glint (i.e. the reflection of the sun radiance on the water surface towards the sensor) is a limiting factor for spill detection. As long as the sun glint does not fully obscure the water underneath, correction can take place to reduce or remove the glint impact¹⁴. Although very thin oil sheens are more easily detected at viewing directions near the sun glint zone, very thick films are more likely to be detected at viewing angles away from the sun without the presence of sun glint. Intense sun glint can be confused with spills or obscure the presence of actual spills. Therefore, an internal sun glint criterion is established and scenes exceeding this criterion are not processed.

Pre-processing of Sentinel-2 imagery includes land masking and correction for adjacency effects¹⁵. Adjacency is the influence of optical light scattered from land or man-made objects. This effect can influence the radiances up to 40km away from the coast and is especially pronounced in areas with low vegetation, but high loose sediment cover as can be found e.g. around the Persian Gulf or the Red Sea. Over open water at mid-latitude and further away from the coast adjacency can be neglected. One of the main factors influencing the radiances of optical satellite imagery is the scattering and absorption that occurs on the way through the atmosphere. Therefore, a precise atmospheric correction considering the local conditions is fundamental. EOMAP uses its own atmospheric correction approach as part of the MIP processing framework applying radiative transfer modelling (RTM)¹⁶. The image corrected this way represents the at surface reflection and serves as basis for the mapping.

Ships and potential slicks are extracted from the imagery, vectorized and classified similar to the workflow previously presented for Sentinel-1. The database consisting of previously processed scenes is then searched and in case of temporarily close matchups

¹⁴ Heege, T. & Fischer, J. (2000): Sun glitter correction in remote sensing imaging spectrometry. SPIE Ocean Optics XV Conference, Monaco, Oct. 16-20.

¹⁵ Kiselev, V., Bulgarelli, B. and Heege, T., (2015). Sensor independent adjacency correction algorithm for coastal and inland water systems. Remote Sensing of Environment, 157: 85-95, ISSN 0034-4257, <http://dx.doi.org/10.1016/j.rse.2014.07.025>

¹⁶ Richter, R., Heege, T., Kiselev, V., Schläpfer, D. (2014): Correction of ozone influence on TOA radiance. Int. J. of Remote Sensing. Vol. 35(23), pp. 8044-8056, doi: 10.1080/01431161.2014.978041

inside an area of interest (AOI), both images and their detections are then compared. As presented before, a whole range of environmental conditions might hamper the detectability or result in false positives. Therefore, at this stage also manual inspection is necessary to reduce the number of false alarms and support the material classification step. Finally, a report is created that is following the EMSA standards including all the relevant information on spill size, location, time and date providing also an indicator on the likeliness for the detection to actually be an oil spill.

TEST CASES

Various oil and chemical spill cases have been studied in and beyond the four pilot case areas. Information on date and location of the spills have been provided by the Maritime and Coastguard Agency (MCGA) of the UK and Cedre. In addition, archives have been searched for past spills with suitable conditions of weather and image availability. During the time of the project no spills were recorded inside the pilot studies. Therefore reported, forwarded and archived spills are located outside the pilot studies but inside the territorial waters of the participating countries.

PHE compiled a list of spills from media reports, which are listed in the Appendix. These incidences have been checked for available imagery and the representation inside those. Unfortunately, no matchups have been found as either the size of the spill was too small to be resolved within 100m^2 pixels, or no images were available imaging the spill.

Information on spills in the British territorial waters in Atlantic and North Sea has also been provided by MCGA and the representation of some of those inside Sentinel-1 VV imagery can be seen in Figure 11. A total of 16 potential spill detections have been provided this way. The shape and size of spills is highly variable, depending on the movement speed of the vessel during release, the time passing by since the release of the chemical and the environmental conditions including wind speed and direction. Spill a) is the smallest of the three presented spills covering 0.27km^2 . This spill is rather compact making it likely that the oil was either released from a slow moving or stationary target or released fast and shortly before imaging time. Spill b) is the hugest spill covering 1.41km^2 consisting of three compact, spatially separated patches. Spill c) exhibits an elongated shape covering 1.13km^2 . Wind speeds in all three cases have been

below 5m/s. Archives have also been searched for potential matchups with Sentinel-2 images. In case of spills a) and b), which both happened on the same day (date and time of image: 2018-06-08 06:30:05 UTC) a Sentinel-2 scene was collected the day after on 2018-06-09 11:21:11 UTC. However, due to the high cloud cover parts of the image are obscured and no spills could be detected in the unobscured parts. Spill c) was recorded within a Sentinel-1 image recorded at 2018-10-15 06:04:13 UTC. A Sentinel-2 scene with little haze and high turbidity levels was recorded at 2018-10-16 11:00:29 but no oil-spills could be detected within the image.

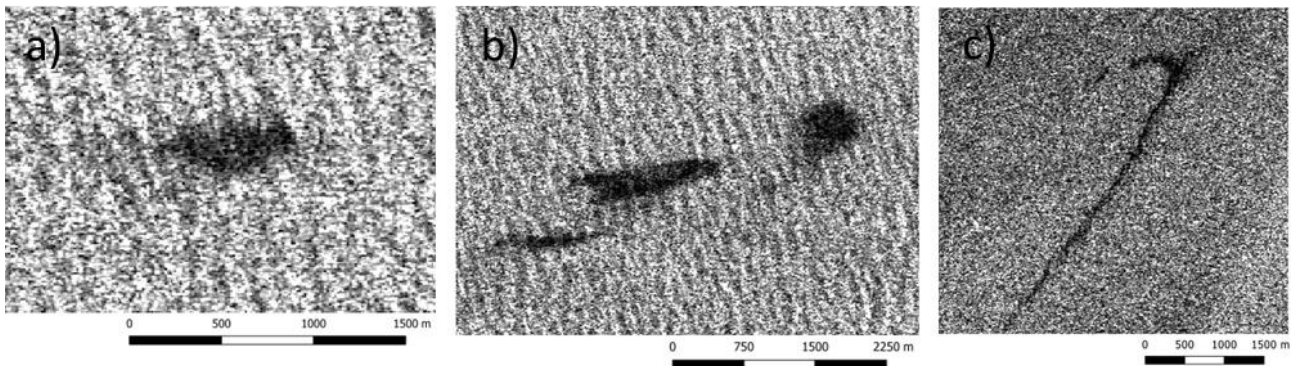


Figure 11: Exemplary hydrocarbon spills in the North Sea and UK waters detected by Sentinel-1 and forwarded by the MCGA.

Adequate image preparation and contrast enhancement is necessary to discriminate the slick area. This is demonstrated in Figure 12 showing the major spill that occurred after the collision of the container ship CLS Virginia and a ro-ro ship north of Cap Corse. The case is especially suited due to the favourable weather conditions with low wind-speed during the spill and the enormous size of the affected area. Imagery from both Sentinel-1 and 2 is available, although not from the same day (8 and 9th October 2018). Vessels can be identified within the Sentinel-1 imagery as bright spots due to the high backscatter of man-made objects. Visible inside both the optical and radar imagery in Figure 12 is the collision of the two ships, with the CLS Virginia being the bigger of the two appearing red in the Sentinel-2 image.

The scenes have been processed according to the workflow presented in the previous chapter. Figure 12 shows the raw unprocessed Sentinel-2 image as an RGB true colour image versus the pre-processed subsurface reflection image after contrast enhancement and atmospheric correction. Subsurface reflection is the radiance just below the water surface. Apart from adjacency effects which are minimal in this case

due to the distance from the land, the image was corrected for atmospheric impacts that occur during the way of the sunlight through the atmosphere (scattering and absorption on atmospheric particles) and effects that occur on the water surface. The movement direction of the spill was west/north-west as can be seen in Figure 13. Note the dark spots in the upper right corner of c) and d). These areas are look-alikes, potentially seaweed or similar and have not been detected as spills.

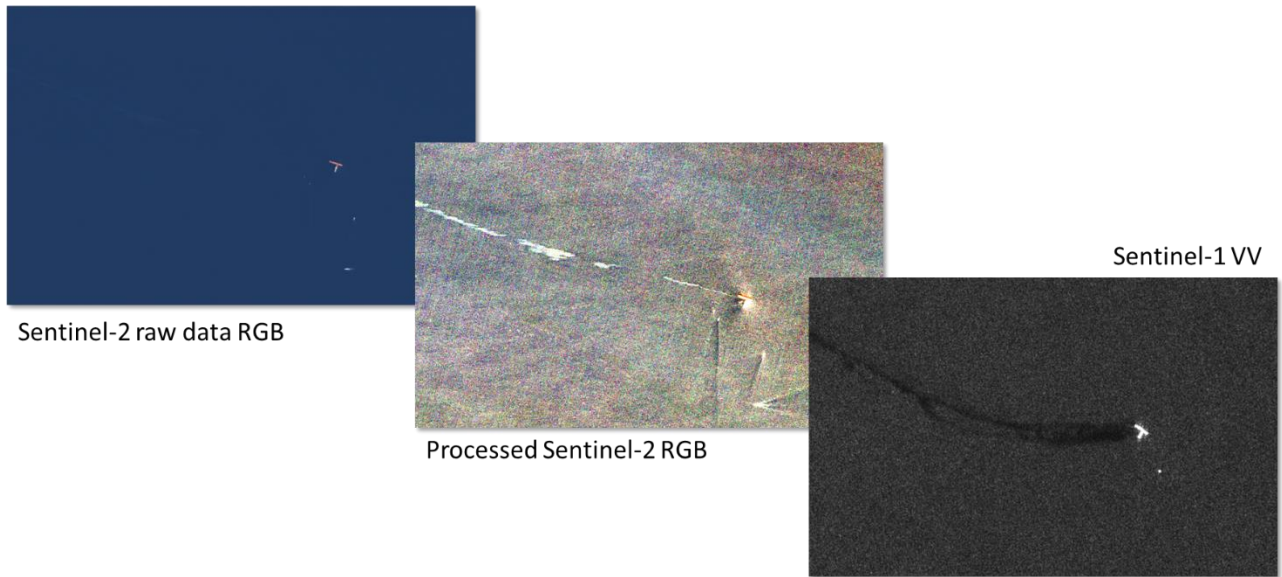


Figure 12: Oil spill after a collision-induced breach in the hull of the container ship CSL Virginia off Corsica on 7.10.2018. Raw Sentinel-2 true color image (RGB) from 9.10.2018 (upper), the same image preprocessed and contrast enhanced (middle) and a Sentinel-1 VV polarization image from the previous day (8.10.2018).

Vectorized spill features are shown in b) and d). In both cases the detection worked well, although the detection on the early stage oil spill is slightly more distinct. On the 9th of October the weathering and splitting of the spill began to proceed more quickly, which makes the detection considerably more difficult. Some areas with low oil thickness at the spill margins have been missed. A precise measure on the omitted areas cannot be given as even within visual analysis the margins between spill and background are not clearly to identify as the transition is fluent. The size of the vectorized spills indicates that on 8.10.2018 the spill covered about 7.7km^2 of water surface and 42km^2 on 9.10.2019. A comparison of the spills at the two dates is given in d), during this time the local wind conditions remained the same and thus the rather slow movement of the spill. In cooperation with Cedre later stages of the spill have also been analysed in order to follow the progression towards the coast. However, after some days the oil settled down into the water column. Although the major part remained within a few centimetres from

the water surface, the oil could not be detected with either Sentinel-1 (as the radar does not penetrate deep enough into the water) or within optical imagery. The case was aggravated by the mixture of oil and seagrass on and short before reaching the coast and future cooperation was agreed to further advance this active field of research.

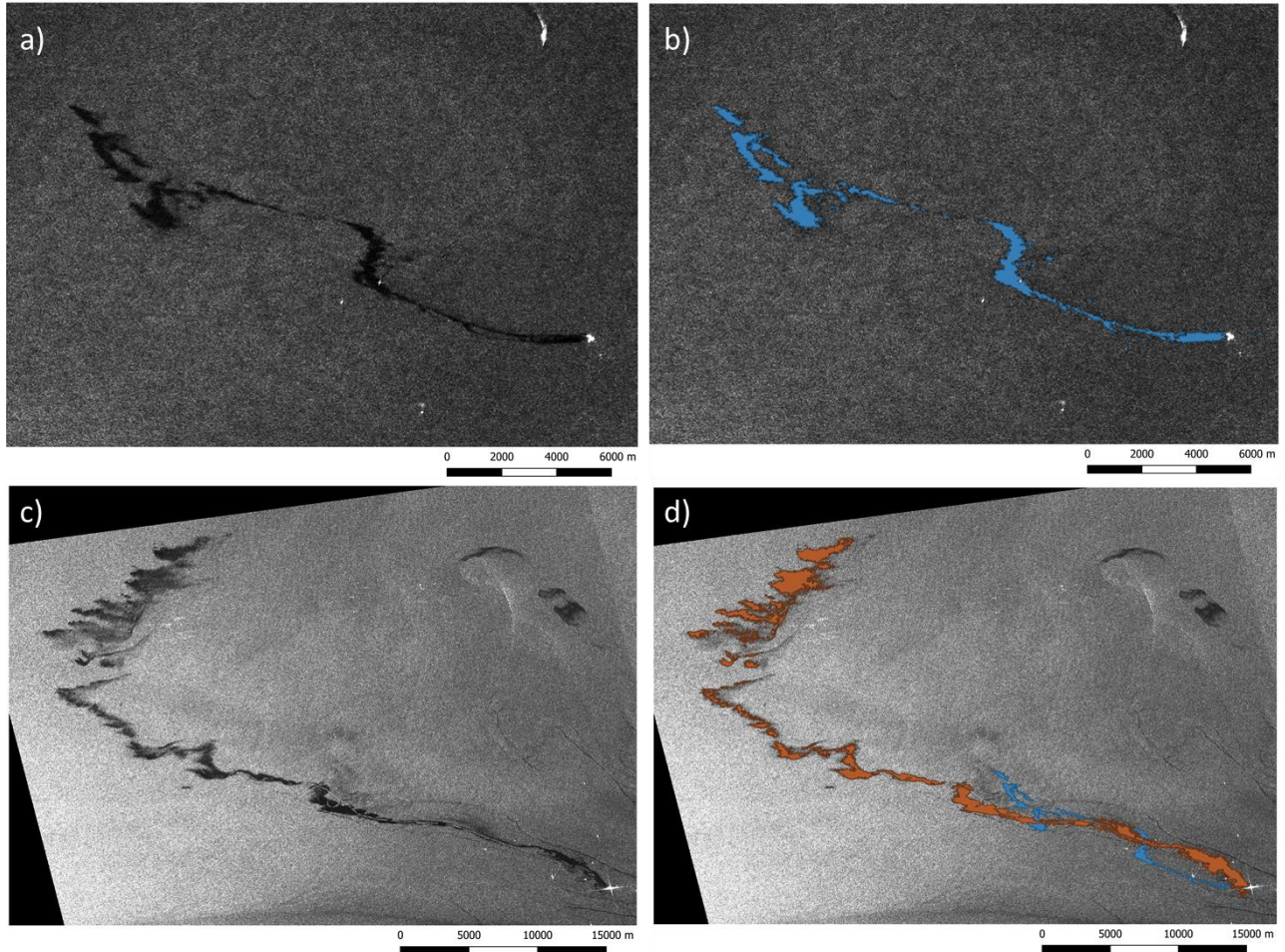


Figure 13: Evolution of the CSL Virginia oil spill as detected by EOMAP's Oil Spill detection algorithm. a) Sentinel-1A image (VV) from 08.10.2018 b) detected extent of the oil spill (7.7km^2) c) Sentinel-1A image (VV) from 09.10.2018 d) detected extent of the oil spill on 08.10.2018 and the day after (42.3km^2).

LIMITATIONS/OUTLOOK

Results of the test cases especially from the CSL Virginia oil spill case, proved promising capabilities of optical sensors to detect large and sufficiently thick layers of oil spills. The additional information layers which can be derived from optical imagery including the spectral bands, derived ratios and GLCM features enhance the oil spill classification framework. Concerning Sentinel-2, especially the visible domain provides valuable contrasting information between oil slick and background. However, certain limitations remain. Oil spills do not exhibit a clearly distinct spectral signature in the visible and

infrared region¹⁷. Also, look-alikes are common in both optical and radar imagery, of which many are even difficult to distinguish with visual inspection and control. Fuzzy rule logic has been applied in research to get more realistic indications for oil spill likeliness, but still certain look-alikes cannot be differed from oil especially within commonly used radar data¹⁸. Therefore, manual interaction of the operator remains necessary also in the presented workflow.

Seldom, optical and radar data are collected sufficiently close such that the application in an emergency response case is limited. The coupling can be used however, to further increase the likeliness of a spill if no immediate measures need to be taken or in case of an ex post analysis.

Although it is well possible to detect ships in both optical and radar imagery, ship tracking information from commercial service providers such as MarineTraffic¹⁹ would further enhance the capabilities of the detection system. Historic tracks could be crossed with detected spills to increase the reliability of a raised alarm and infer the source of the spill.

The thickness of the oil layer is an important information for responding entities in order to initiate adequate counter measures. As SAR imagery cannot provide information on oil thickness, optical imagery and the NIR bands were used in the past to estimate oil thickness²⁰. Microwave radiometers and laser fluorosensors can provide supplementary information about the type and amount of oil. These instruments are not available on satellite sensors with sufficient resolution, but they are used on surveillance aircrafts.

¹⁷ Fingas, M., Brown, C. (2014): Review of oil spill remote sensing. *Marine Pollution Bulletin*. DOI: <http://dx.doi.org/10.1016/j.marpolbul.2014.03.059>

¹⁸ Kolokouassis, P., Karathanassi, V. (2017) : Oil Spill Detection and Mapping Using Sentinel 2 Imagery. *J. Mar. Sci. Eng.* 2018, 6, 4; doi:10.3390/jmse6010004

¹⁹ <https://www.marinetraffic.com>

²⁰ Clark, R.N., Swayze, G.A., Leifer, I., Livo, K.E., Lundeem, S., et al., 2010. A method for qualitative mapping of thick oil using imaging spectroscopy. United States Geol.Survey, <<http://pubs.usgs.gov/of/2010/1101/>>.

Optical remote sensing of oil spill remains an active field of research. Upcoming or not yet accessible hyperspectral missions such as the German ENMAP and the Italian PRISMA mission are promising for an increased sensitivity in detection and discrimination of relevant chemical substances.

Pilot Cases

The activities of this work package focus on four project case study areas including transitional waters. The extent of these sites was such that areas under risk of flooding are covered by the mapping. Therefore, project partners and local authorities were questioned, and their expertise used to define the exact outline of the areas of interest.

STUDY AREAS

The case studies (Figure 14) have different conditions regarding factors such as tidal range, sediment load, shape of the estuary and bathymetry. The Severn river entering the Bristol channel has the highest sediment load and turbidity (Table 2). While turbidity can also reach high levels in the Loire estuary, the sediment load is more variable and does not exhibit a constantly high load throughout the year. The Severn is also the hugest pilot case covering almost 3400km² of which 2500km² are covered with water at high tide. The area features one of the highest tidal ranges in the world, exposing large portions of land on low tide. Contrary conditions are found in the Spanish pilot study in the Galician Ria of the Rio Ulla river. While the tidal range is low, water level variations are enhanced by interseasonal variation and dry periods in summer as well as prolonged rainfall and flooding hazard in the wet season. The Tagus pilot site includes three of the municipalities most affected by flooding in the greater Lisbon area including the Lisbon, Loures and Odivelas municipalities.

Table 2: The 4 pilot case areas and the area monitored.

Study area	Country	Size [km ²]	Tidal range [m]	Sediment load
Severn	United Kingdom	3390	10	Very high
Loire	France	2246	6	High
Tagus	Portugal	3300	4	Moderate
Rio Ulla	Spain	224	3	Low

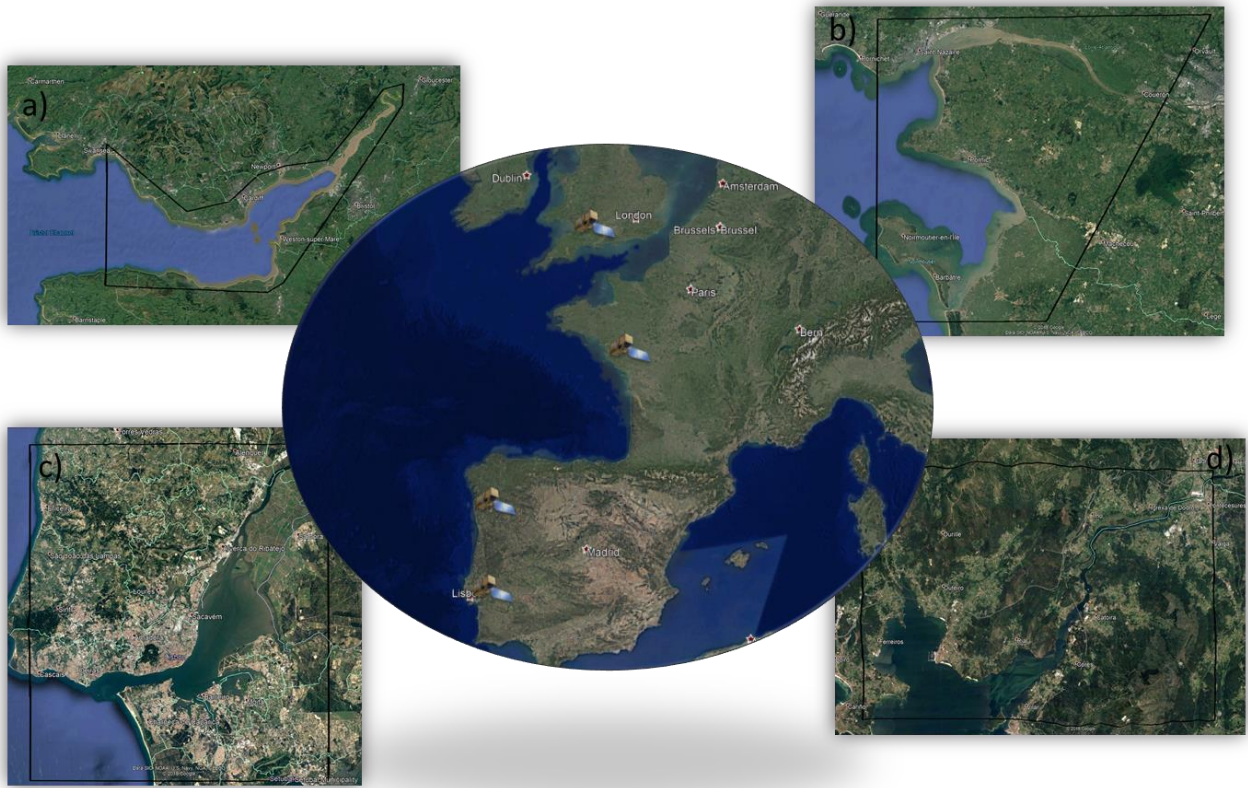


Figure 14: Locations of the study areas. a) Severn estuary, UK b) Loire estuary, France c) Tagus estuary, Portugal d) Rio Ulla estuary, Spain.

Several study sites cannot be covered by a single image acquisition due to their extent. Figure 15 shows the coverage of the Tagus river study site by Sentinel-2. In total 18 satellite images are necessary to cover all four pilot case studies with all sensors. Over the course of a year, this amounts to about 1350 images of Sentinel-2 in all pilot case studies as well as 92 Landsat 8 images (Table 3). A complete coverage with Sentinel-2 per region of interest is expected to be achieved 146 times a year in Severn, Tagus and Rio Ulla. 182 images are taken within a single year in the Sentinel-2 tile 30TWT over the Loire estuary, however a completely covering image is taken only 146 times a year. Although, each satellite image is processed separately and several scenes are required for full AOI coverage, each study site is fully covered by each sensor on a single day.

Table 3: Landsat 8 path/rows, Sentinel-2 tiles and the number of potential images per year at each pilot case study.

Study area	Landsat 8 path/row	Sentinel-2 Tile	Images per year	
			Landsat 8	Sentinel-2
Severn	203/24	30UWC, 30UVC, 30UVB	23	438
Loire	201/27	30TWT	23	182

Tagus	204/33	29SMD, 29SND, 29SMC, 29SNC	23	584
Rio Ulla	204/30, 205/30	29TNH	23	146



Figure 15: Sentinel-2 coverage of the Tagus river estuary. Left: Single image tiles, 4 Sentinel-2 tiles are needed to cover the whole area. Right: Extent of the single tiles (green) over the Tagus river AOI (black rectangle).

The monitored areas have been defined in cooperation with the project partners and local entities. As for the Tagus river estuary in Lisbon, also the other AOIs cover those areas most heavily affected by flooding in the transitional water region based on past events. Figure 16 shows the areas at risk of flooding in the Loire estuary, from the river mouth close to St. Nazaire (to the left, outside of the map) to Le Pellerin, which is only a few kilometres away from the densely populated area surrounding Nantes. No settlements are located inside the dark blue coloured zone of strong risk, but at least four settlements are situated at the margins and inside the extended risk zone (Paimboeuf, Corsept, Cordemais, Lavau sur Loire). Also, inside the strong risk zone is the power plant of Cordemais, directly situated on the Loire riverbank. The monitoring provides data of these areas at risk, supplying local entities with additional tools for planning and risk management.

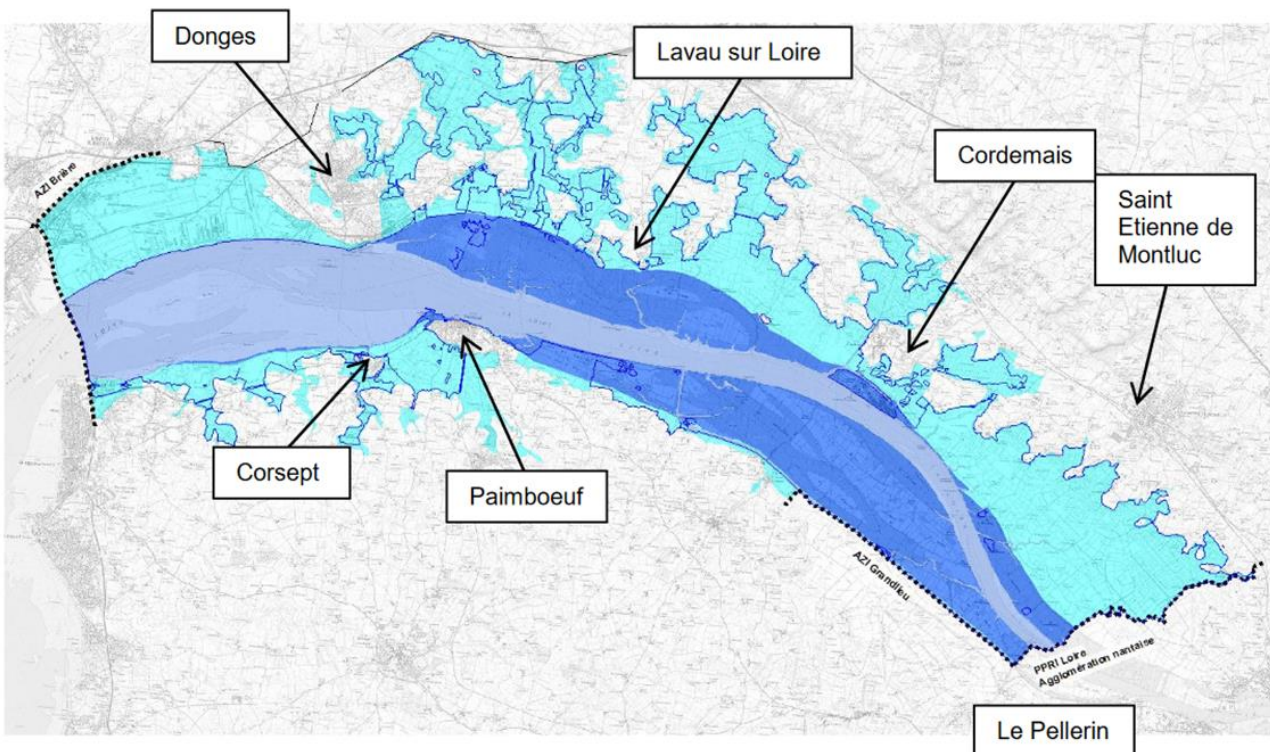


Figure 16. Overview on the inundation zones in the Loire estuary as defined by hydrogeomorphology. Areas in light blue are under moderate risk, areas under dark blue are at strong risk (source: Cedre).

PILOT CASE STUDIES: DISCUSSION OF RESULTS

This chapter presents a selection of results from each of the four pilot studies. In total more than 200 satellite scenes have been processed in order to adjust the workflows and calibrate them on the local environmental conditions. For example, in Galicia sun glint is a dominant phenomenon thus a higher level of correction was necessary, while in the Severn estuary turbidity levels were so high that the land-water masking settings had to be adjusted for a proper differentiation.

Results from the oil and chemical spill detection are not presented in this chapter as the study cases are not located inside the pilot case studies. Refer to the Test Cases chapter.

SEVERN

The Severn pilot study is not only the hugest monitored area, but also the most extreme regarding tide, turbidity levels and cloud cover. For this reason, Sentinel-1 is an especially valuable addition to the optical imagery in order to monitor the water cover throughout the whole year and during the almost completely clouded seasons. Two Sentinel-2 scenes in 2018 and early 2019 were found and processed, which were almost

completely cloud free. One of the two scenes is shown in Figure 17. In the WEX and TUR products, clouds are masked with white colour. After fine tuning the land-water masking also heavily sediment laden parts of the river are detected as water. NTU values at this day in July 2018 with a Sentinel-2 scene taken at high tide can reach values higher than 200 FTU. The water becomes increasingly less turbid further out towards Cardiff when the waters of the Severn start to mix up with the Atlantic Ocean.

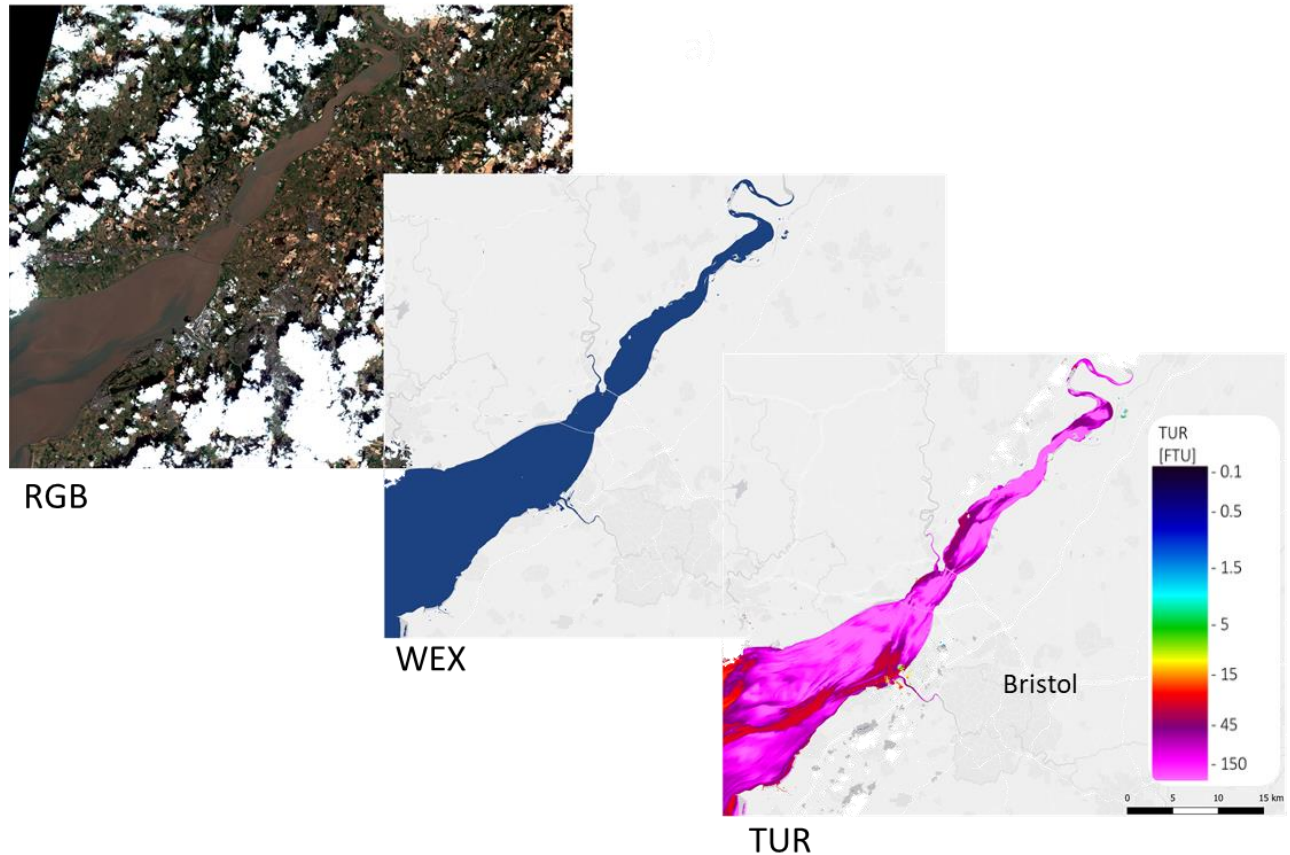


Figure 17: RGB, WEX and TUR derived from a Sentinel-2 scene collected on 2018-07-31. Note the high levels of turbidity, which are almost constant throughout the year.

The high tidal variation inside the Bristol channel is an important variable to consider for the modelling of flooding cases and water dynamics in the area. Figure 18 shows the water level and coverage at two tidal stages in the Bristol channel close to Bristol. For a better visual impression, the topography has been strongly vertically exaggerated. Black colours indicate the flood plains, which are close sea level and exhibit an almost flat topography likely prone to flooding. The topography increases further away from the channel up to 150m a.s.l. At lower tides, huge areas are exposed especially further up the Severn river. Note that in the presented case, tidal differences are rather small (3.5m) while the maximum differences in the Bristol channel can amount to 15m. During

heavy rainfall invents, the water level can also vary due to the water inflow from major secondary tributaries such as the river Avon that flows through Bristol.

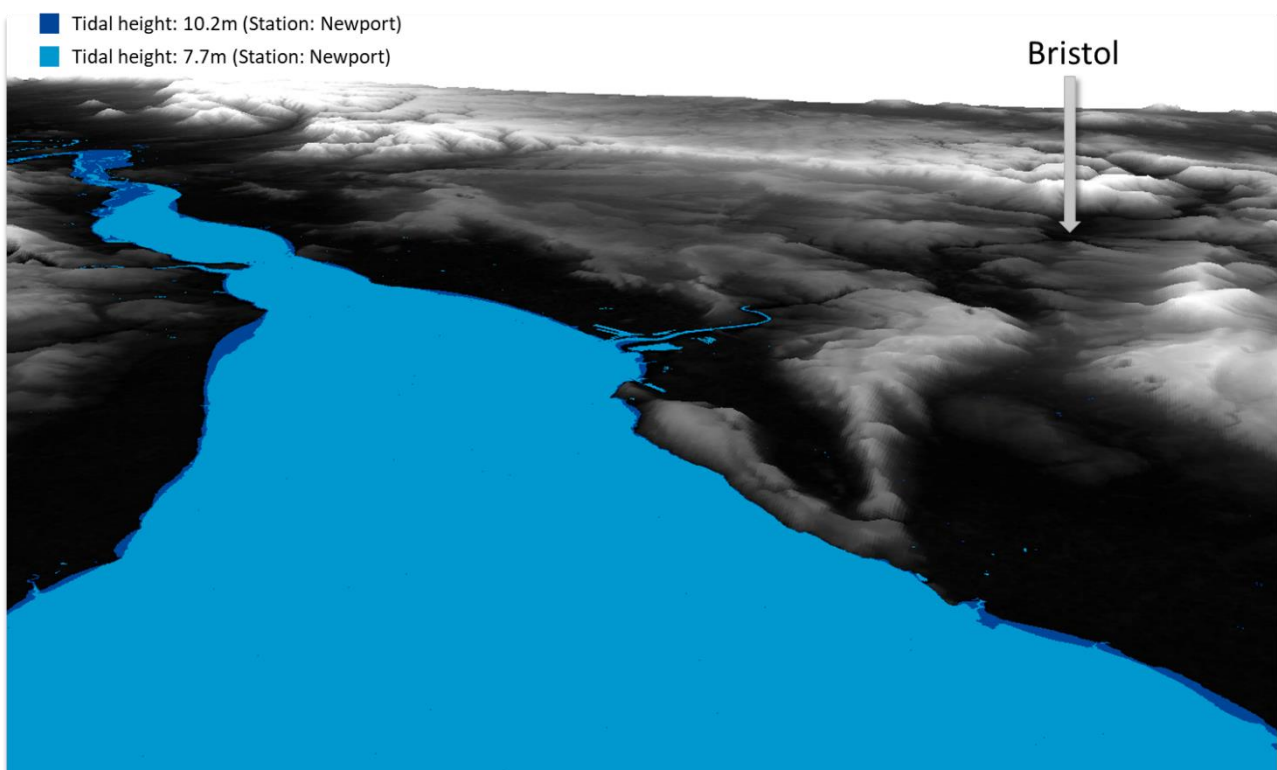


Figure 18: Topography (strongly exaggerated) from SRTM DEM at the Bristol channel close to Bristol overlain by the water level at different tidal stages measured at station Newport.

Water stages at different tidal level and the areas potentially exposed at lower tidal stages are also important to know for the local ship traffic and waterway management. In Figure 19 the Avonmouth harbour and the inflow of the Avon river are an example for the difficult tidal environment. While the main riverbed remains continuous throughout the two scenes, large tidal flats are exposed at the river mouth. The Avon does not flow straight into the Bristol channel, but describes a bow around the tidal flat in the south. Continuous monitoring is necessary in such a case, because structures in the tidal flats often change position and do not remain stable over time as hard bottom does. Ongoing sedimentation and main channel shifting also occur further inlands at the inflow of the Severn into the Bristol channel.

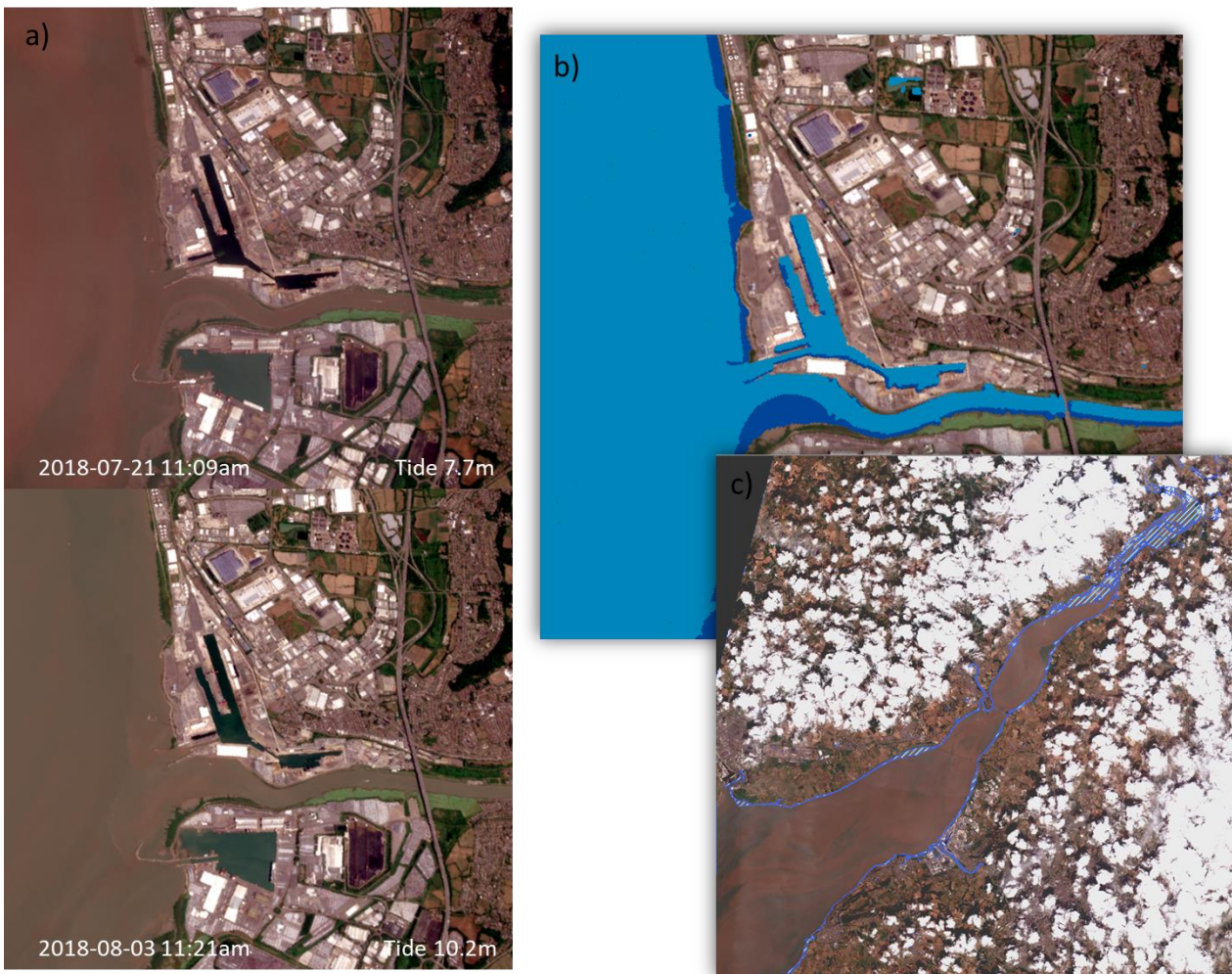


Figure 19: a) and b) water coverage at different water stages at the Avonmouth harbour. c) Differences between 7.7m tide and 10.2m in the Severn estuary.

LOIRE

The Loire pilot case study comprises a range of different turbidity regimes with a tidal influence weaker than in the Bristol channel but still strong and more than 6m. In Figure 20, time series plots from six locations inside the AOI are shown. The differing number of observations can be explained by the masking of these areas within some scenes due to clouds, exposure of land through tidal variation or unsuitable recording geometry. Point 1 clearly has the strongest turbidity throughout the year due to the high sediment transport within the Loire and the constant water motion and mixture at the river inflow. Sediment load strongly decreases further outside on the estuary as the clearer water from the Atlantic Ocean starts to become the dominant water type. The influence of season can also be seen within Point 2, at which the turbidity decreases from winter to summer. A similar although less pronounced pattern is visible at Point 3, which is

located even further outside. This shows that seasonal variation is determined mainly by the sediments transported into the estuary through the Loire river. Points 4, 5 and 6 show the input of sediments through tidal motion. Closer to the coast where sediment suspension is strongest, turbidity remains stable throughout the years and no clear pattern can be determined. No major rivers enter the coast at the bay south of the Loire estuary, wherefore no seasonal variation can be found, and turbidity variation is explained almost completely through tidal influence. With increasing distance from the coast decreases from values above 20 NTU at Point 6 to below 15 NTU at Point 5 and below 5 NTU at Point 4 which is located farthest away from the coast.

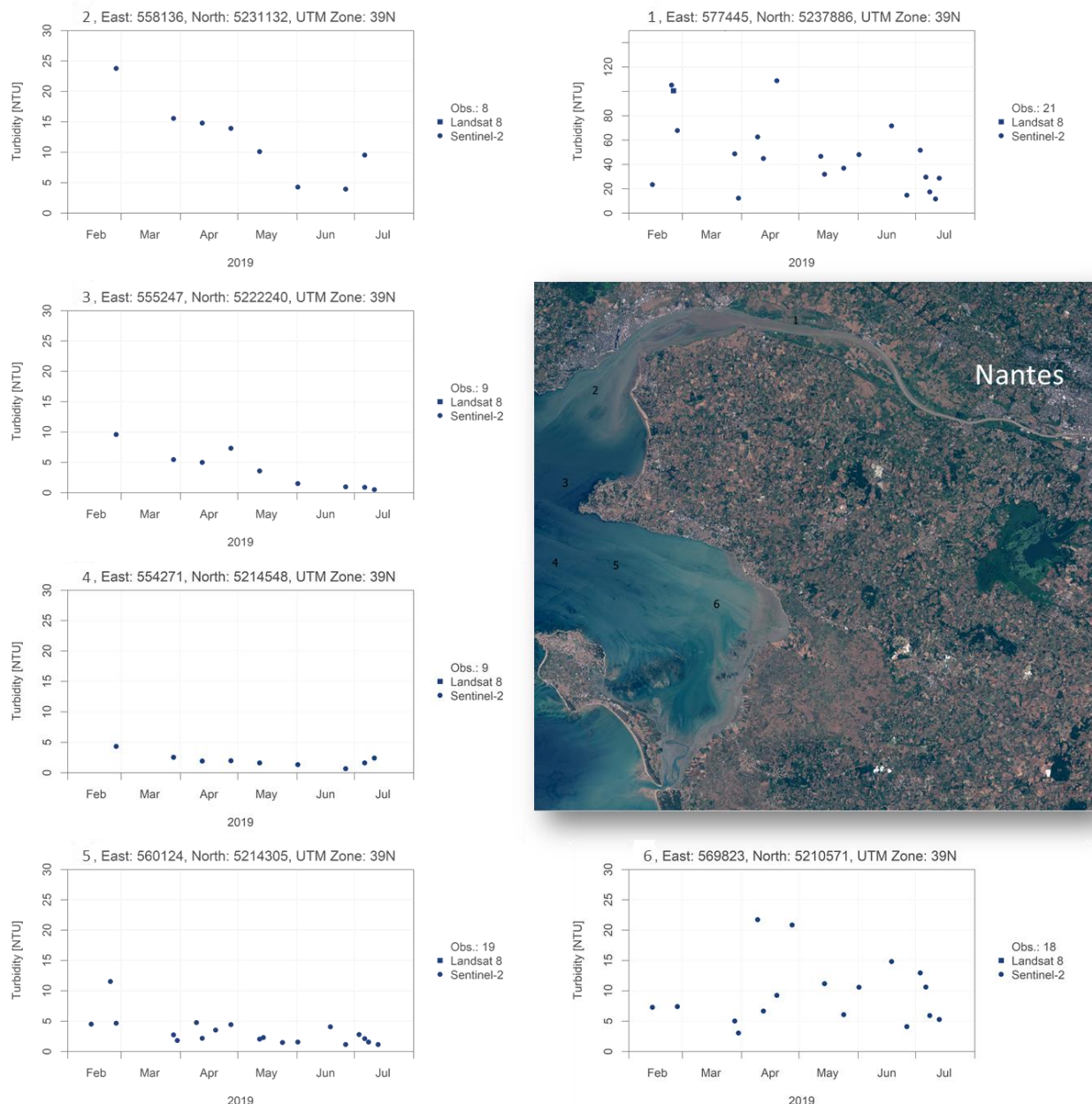


Figure 20: Different turbidity regimes at the inflow of the Loire into the Atlantic Ocean.

How far sediments are transported into the Atlantic Ocean is determined by weather and water flux conditions but also by the input from the Loire river. As the input of sediments is higher when the precipitation is higher, more sediments are transported into the ocean in autumn and spring times. In Figure 21, heavily sediment laden waters reach further into the ocean early in the year and at the end of the year. As precipitation in the hinterland was strongly decreased during the warm summer in France 2019, sediment input decreased from February to June.

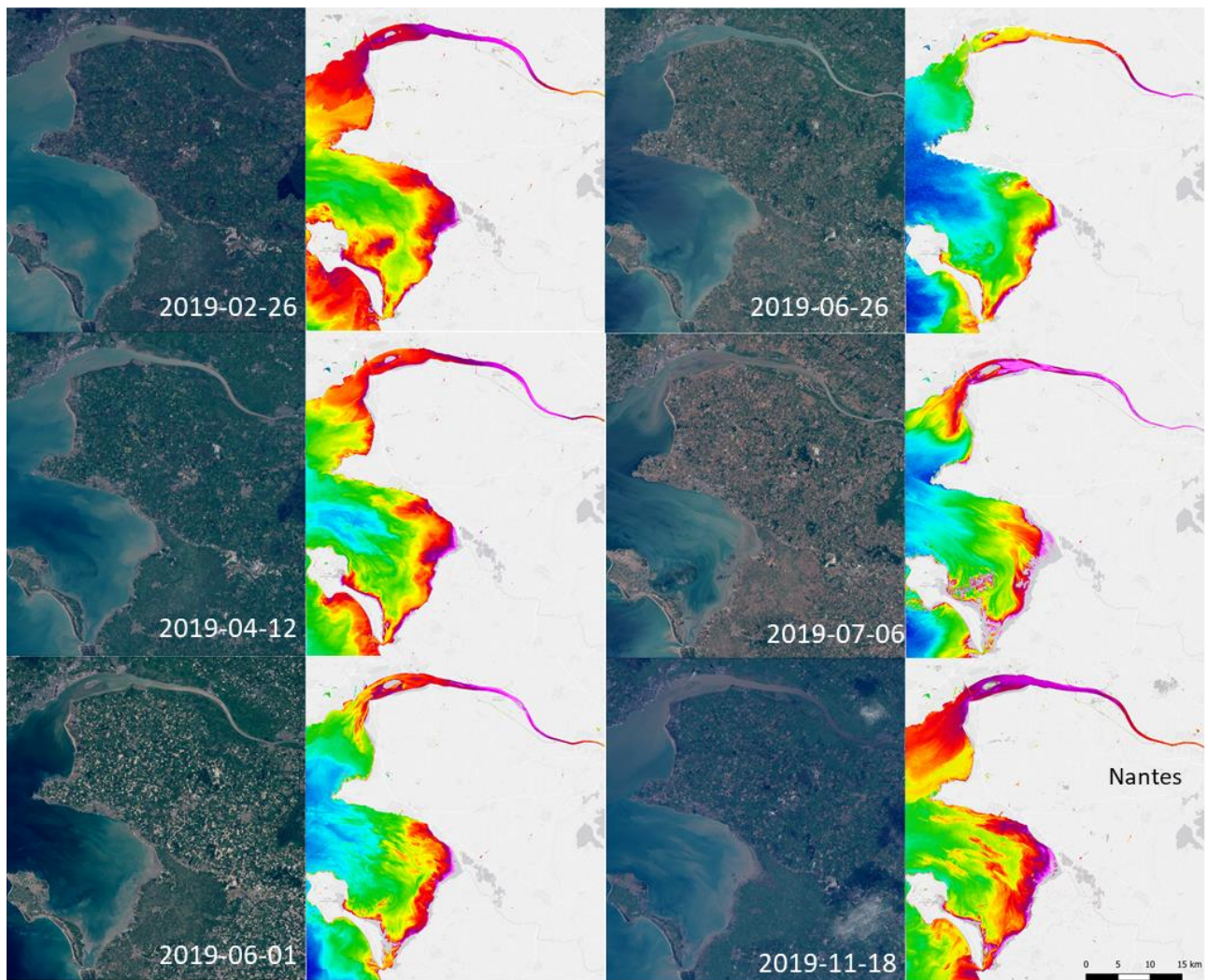


Figure 21: Seasonal variation of turbidity into the Loire estuary. Images from Sentinel-2.

TAGUS

The Tagus estuary is almost completely surrounded by human settlements. Large parts of the area especially further inland are only a few meters above the sea level. The Tagus estuary and the Atlantic Ocean are connected via a rather thin inflow that is about 1.5km wide at its narrowest place. This geometry results in a turbidity plume into the Atlantic

Ocean, which is clearly visible inside satellite imagery (Figure 22). The differentiation between sediment laden river waters and the clear Atlantic waters is especially strong as the turbidity is not dispensed on a wide area as it's the case in the Loire and Severn estuaries. Figure 22 also shows a comparison between the spatial resolution and the level of detail that can be resolved within the two optical sensors used for turbidity calculation. The resolution of Sentinel-2 is 9 times higher than that of Landsat 8, resulting in a more distinct coastline at the small beacon island in front of the Tagus river mouth.

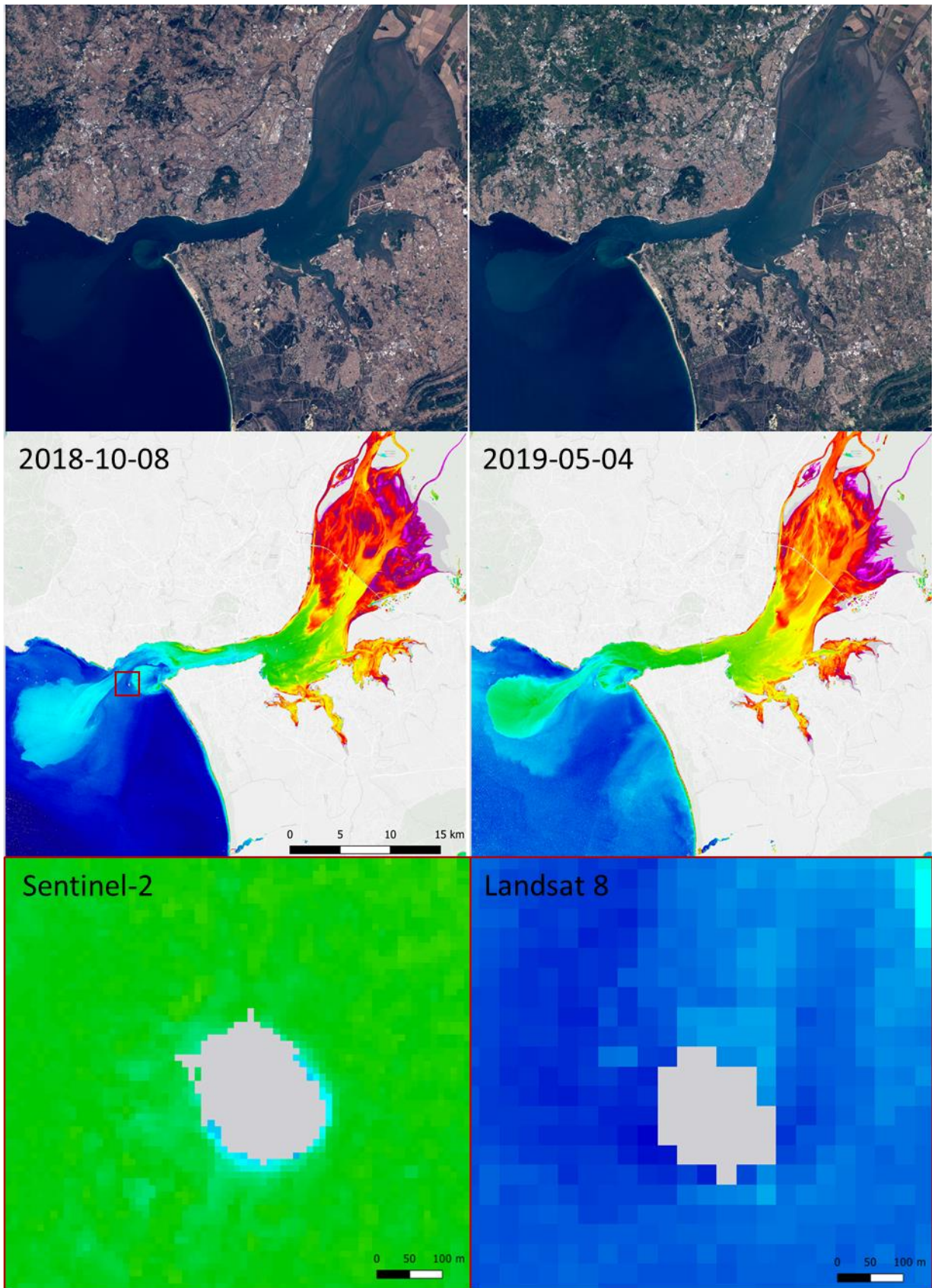


Figure 22: The turbidity plume of the Tagus river. The red rectangle marks the area used for a comparison of spatial resolution between Sentinel-2 and Landsat 8.

In order to support the modelling done as part of WP2, EOMAP agreed on deriving a shallow-water bathymetry (SDB) map at the Tagus river estuary as part of the project (Figure 23). The SDB comprises the very shallow water areas below 2.5m depth which are especially important for the coastal modelling. The SDB was used by IST in order to calibrate their models on water/river depth.

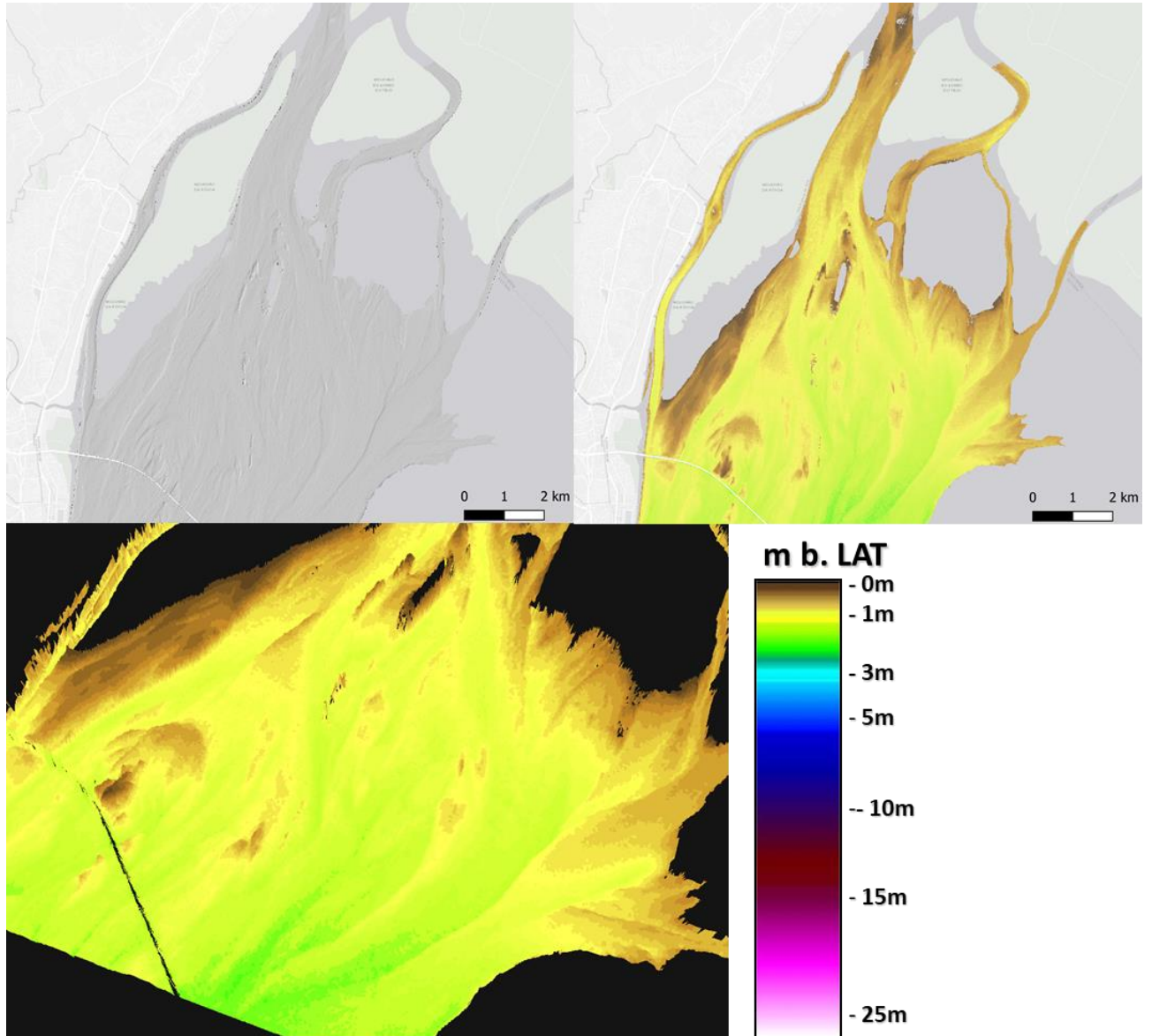


Figure 23: Satellite-Derived Bathymetry (SDB) at the Tagus river estuary. The bathymetry focusses on very shallow water areas of maximum 2.5m depth. Upper left is the hillshade model of the SDB, which is displayed in 2-D on the upper left and 3.D below.

RIO ULLA

The Rio Ulla is the smallest pilot case and the smallest estuary studied. As the tidal range is rather low compared to the others, much variation in water level is explained by interseasonal variation and decreased rainfall during the summer period. This can be

seen in Figure 24 where the lowest water coverage at similar tidal stage is in May. Usually starting in October, rainfall starts to increase in Galicia. At the river inlet to the right, sandbanks are exposed during the low water stages.

The Galician environment is challenging for water quality retrieval due to the strong influence of sun glint. As described in the previous chapter, sun glint can be corrected as long as a sufficient signal is originating from below the water surface. Turbidity in the Rio Ulla estuary is rather low compared to the other study sites. FTU values mostly range between 0.1 and 5. The amount of sediments transported into the estuary increases during the rainy season as can be seen in the turbidity image from October in Figure 25. Note that higher turbidity values in the Rio Ulla inflow originate from confusion with ground. As described in the Turbidity chapter, no discrimination can be made between optically shallow waters and turbidity. In the case of the Rio Ulla estuary, these areas have not been masked as optically shallow, because they potentially become optically deep during flooding conditions or after high rainfall.

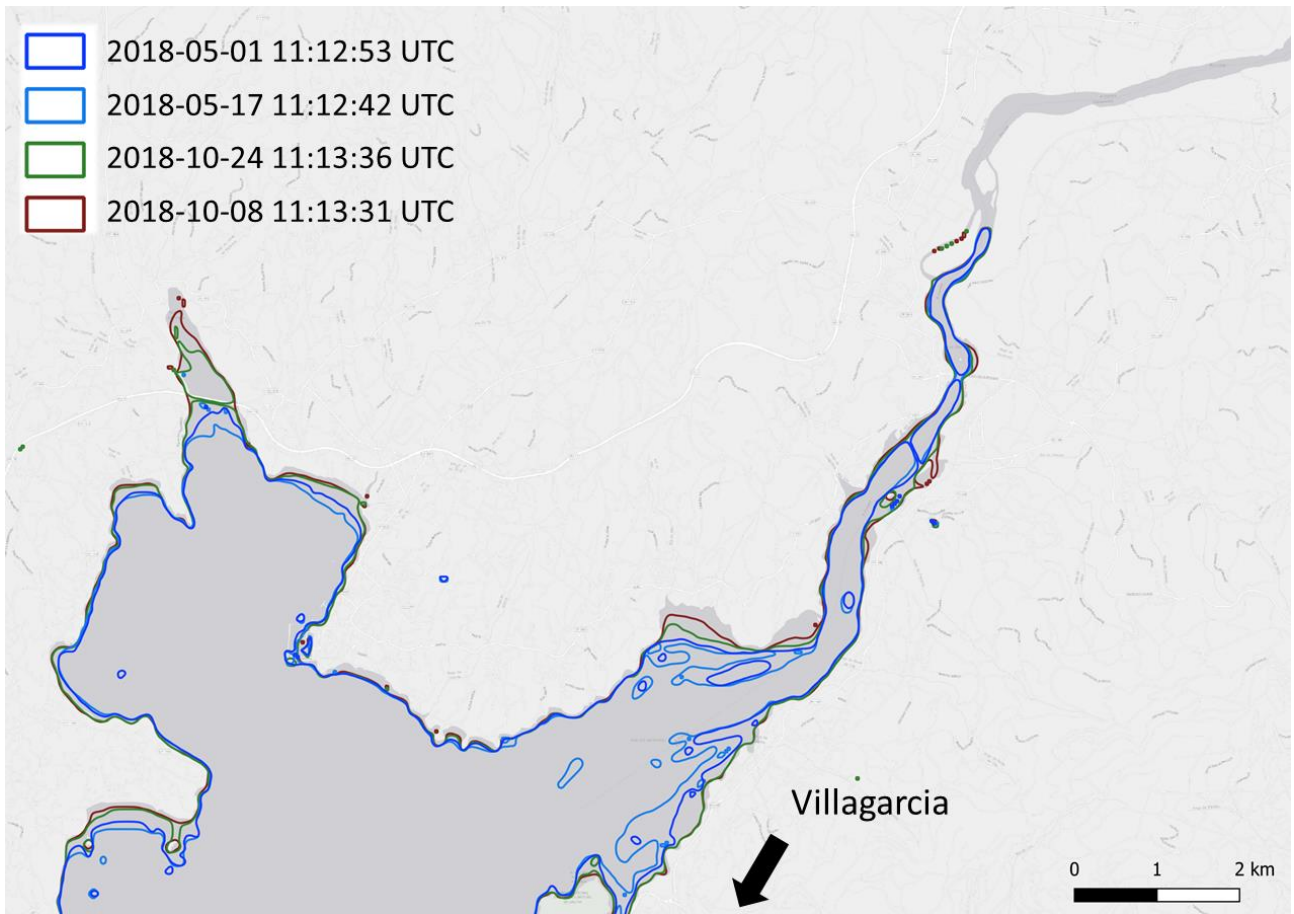


Figure 24: Water coverage in the Rio Ulla estuary at similar tidal stages but different times of the year.

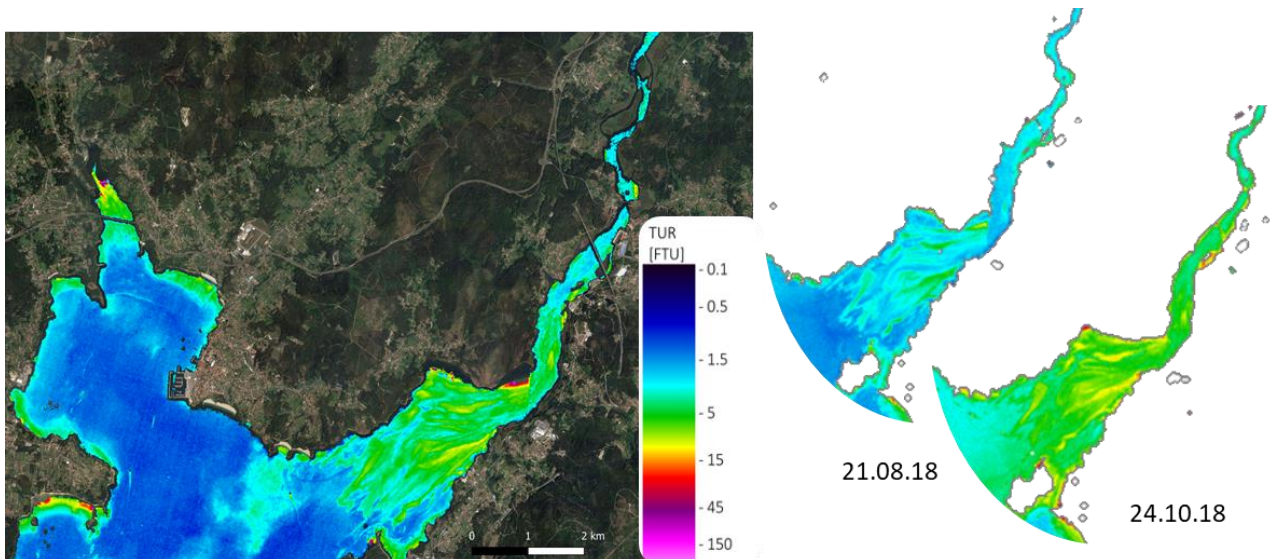


Figure 25: Turbidity in the Rio Ulla estuary. The image to the left was collected on 2018-08-26, all data derived from Sentinel-2.

Quality Control

As a standard output of the water quality processing, an accuracy or quality indicator, is calculated for each retrieved parameter and for each detected water pixel. This measure comprises a comprehensive range of factors that can impact the derived product quality, including:

- the geometry between sun, target, and sensor
- the estimated sun glint probability
- the retrieved aerosol optical depth
- residuals of the measured and modelled sensor radiances and subsurface reflectance
- the comparison of retrieved water species concentrations to extreme values as defined in the configuration files
- pixels affected by cloud shadow
- shallow water areas

Threshold values define distinct values when a parameter is assumed to influence the quality. All parameters are integrated into one remaining quality parameter, allowing both an improved flagging and a quality weighting of pixels, that can later be merged into integrated 3rd-level products.

The quality information is part of each standard geodata delivery and is visualized by two different 8bit GeoTIFFs:

- QUT - Total Quality, quantifying the overall quality of each pixel from low to high. Only valid water pixels - excluding land, cloud or flagged pixels - are represented in the QUT indicator (see Figure 26).

- QUC – EOMAP Quality coding, revealing the processor's internal quality check, split into the defined indicators (e.g. sun glint, shallow water risk, etc.). These are classified into 'no quality concerns', 'quality risk' and 'bad quality' (flag). Note that 'quality risk' pixels are marked as such but not flagged (see).
- The QUC file indicates the main quality influencing parameter using a specific EOMAP quality coding classification scheme with corresponding grey values (GV), shown in Figure 26.

Professional version allow combination of the two most relevant flags:					
First number = most relevant flag					
1-digit-number refer to second relevant flag, e.g. 1 for sunglint risk, 2 for large solar zenith angle					
Examples:	25 Warning flag for large zenith solar angle and Whitecaps 114 Critical flag for sunglint, plus warning for aerosol above limits				
GV	GV range	Flag status	Flag description	Color code	Color
0	0	Water	No risk identified	0 0 0	
10	10 - 19	Warning	sunglint risk	148 138 84	
20	20 - 29	Warning	large solar zenith angle	83 141 213	
30	30 - 39	Warning	large spacecraft zenith angle	218 150 148	
40	40 - 49	Warning	Aerosol above limit or Cirrus risk	196 215 155	
50	50 - 59	Warning	Cloud Shadow	177 160 199	
60	60 - 69	Warning	Shallow water risk	146 205 220	
70	70 - 79	Warning	Mixed pixel risk	250 191 143	
80	80 - 89	Warning	Retrieved concentration at configuration limit	190 190 190	
90	90 - 99	Warning	Retrieval / processor warning	210 210 210	
110	110 - 119	Critical	sunglint risk	73 69 41	
120	120 - 129	Critical	large solar zenith angle	22 54 92	
130	130 - 139	Critical	large spacecraft zenith angle	150 54 52	
140	140 - 149	Critical	Aerosol above limit or Cirrus risk	118 147 60	
150	150 - 159	Critical	Cloud Shadow	96 73 122	
160	160 - 169	Critical	Shallow water risk	49 134 155	
170	170 - 179	Critical	Mixed pixel risk	226 107 10	
180	180 - 189	Critical	Retrieved concentration at configuration limit	120 120 120	
190	190 - 199	Critical	Retrieval / processor warning	130 130 130	
220	220	No value	Transition Zone	102 255 51	
221	221	Unreliable	Shallow water automatically	146 205 220	
222	222	Unreliable	Shallow water manually	60 159 186	
223	223	Unreliable	Floating material	32 95 107	
230	230	No water	Land	102 255 51	
232	232	Unreliable	Invalid pixel manually	255 192 0	
240	240	No water	Cloud	255 255 255	
242	242	Unreliable	Cloud Shadow manually	96 73 122	
244	244	Unreliable	Hill shadow	73 57 93	
250	250	No retrieval	No retrieval / out of AOI or image extend	255 0 0	

Figure 26: EOMAP QUC quality coding

An example for a flag value is the so called “transition zone”. Because of the spatial extent of the single pixels (e.g. 10x10m in case of Sentinel-2), it is likely that spectral mixing of signals from land and water within a pixel occurs in a transition zone. This would lead to unreliable retrieval results. Therefore, an algorithm masks out these regions automatically during processing. A high-resolution land-water-mask is used to

determine the land-water boundary, which is then filtered to create this transition zone. In the 8bit product, this transition zone has a value of 251, in the QUC product the transition zone has a value of 220).

Setup of Monitoring Systems

A total of 12 fully automated monitoring systems have been established in the 4 pilot case studies. The systems do not need any operator interaction and provide RGBs, WEX and TUR to the user via the HazRunOff webtool depending on the size of the pilot study and sensor resolution. Processing for Landsat 8 takes 1.5-2h from the time the scenes are available online to the time the products are readily available on the webtool. Due to the 9 times higher resolution processing for Sentinel-2 takes longer, depending on the study area between 3-4h. As only WEX is derived from Sentinel-1, these products which are most requested in case of flooding can be provided within 0.5-1h after data availability.

DATA SELECTION

Out of several available and archived satellite recordings, we automatically select datasets with the following priorities:

- cloud and haze free conditions
- water clarity as good as possible
- little or no impact on sun glint (mirror-like reflectance of the water surface)
- little or no impact of waves and wave-breaking.

If the cloud cover exceeds a pre-defined value of 50% the scene is not downloaded and processed. This restriction only applies to the optical imagery due to the cloud penetration of the radar system.

AUTOMATED DATA ACCESS FROM ARCHIVES

For the automatical download of Sentinel-1A/B, Sentinel-2A/B and Landsat 8 we selected the AWS environment²¹ due to best performance and easiest access.

As next step, Python based scripts have been written to automatically search through these archives in order to have an operational download in place. The tools run time-triggered query searches through these archives for new data in form of so called cronjobs. Combined with the operational EOMAP workflow system EWS, water quality processing is automatically initiated on EOMAP servers for the two reservoirs.

When running the script, a set of parameters can be specified in the query, partly mandatory (m) or optional (o):

- Output directory (folder) (m)
- Path/row (Landsat) or tile identifier (Sentinel-2) (m)
- Start and end date (o)
- Cloud coverage (o)

Note that in the Rio Ulla pilot study only the ascending pass of Sentinel-1 is used as the descending pass exhibits a geolocation offset in the GRD product.

Integration in the HazRunOff Webtool

The HazRunOff webtool (WP3) is the interface for information flow in the project. It combines data from modelling (WP2), in-situ measurements (A1.2), airborne sensors (A1.3) and remote sensing (A1.1). The webtool is promoting faster decision making through dashboards, timeseries charts of measured and modelled data, tools to run simulations and a WMS interface. Data from remote sensing as part of this activity are seamlessly ingested into the WMS service, allowing for fast query and visualization of the derived products.

²¹<http://sentinel-s1-l1c.s3.amazonaws.com>, <http://sentinel-s2-l1c.s3.amazonaws.com>, <https://landsat-pds.s3.amazonaws.com>

AUTOMATED PRODUCT UPLOAD USING GEOSERVER API

GeoServer will be used to store and query the EO based data sets for display in the HazRunOff webtool.

To establish communication between the EOMAP processing chain and the GeoServer, GeoServers Representational State Transfer Application Programming Interface, short REST API, is used. With Python based tools, the output water quality products in form of 8bit (RGB and WEX) and 32bit GeoTIFFs (TUR) are automatically uploaded to the GeoServer, hosted by EOMAP. At this stage, currently the following layers are created:

Table 4: Current layers in GeoServer for the HazRunOff project

Name	Content	Resolution [m]
es_ulla_rgb_daily	RGB images from Landsat 8, Sentinel-1 and 2. Rio Ulla estuary	10, 30
es_ulla_wex_daily	WEX images from Landsat 8, Sentinel-1 and 2. Rio Ulla estuary	10, 30
es_ulla_tur_daily	TUR images from Landsat 8, Sentinel-2. Rio Ulla estuary	10, 30
gb_severn_rgb_daily	RGB images from Landsat 8, Sentinel-1 and 2. Severn estuary	10, 30
gb_severn_wex_daily	WEX images from Landsat 8, Sentinel-1 and 2. Severn estuary	10, 30
gb_severn_tur_daily	TUR images from Landsat 8, Sentinel-2. Severn estuary	10, 30
pt_tagus_rgb_daily	RGB images from Landsat 8, Sentinel-1 and 2. Tagus estuary	10, 30
pt_tagus_wex_daily	WEX images from Landsat 8, Sentinel-1 and 2. Tagus estuary	10, 30
pt_tagus_tur_daily	TUR images from Landsat 8, Sentinel-2. Rio Ulla estuary	10, 30
fr_loire_rgb_daily	RGB images from Landsat 8, Sentinel-1 and 2. Loire estuary	10, 30

fr_loire_wex_daily	WEX images from Landsat 8, Sentinel-1 and 2. Loire estuary	10, 30
fr_loire_tur_daily	TUR images from Landsat 8, Sentinel-2. Loire estuary	10, 30

The data products are stored also physically in the GeoServer infrastructure. To keep the information accessible through the webtool up to date and relevant for the user group, products older than 30 days are automatically removed from the server. With Bentley Systems' integration of the products into the website, the data can be searched and visualized in a Web Mapping Service (WMS) environment.

VISUALIZATION IN THE HAZRUNOFF WEBTOOL

Remote sensing derived data in the HazRunOff webtool can be accessed through the **Map** menu (Figure 27). To visualize the information in a study site, choose the domain (currently one of Spain, France, UK, Portugal), the remote sensing product to display and the imaging time via **Instants**. Three products are available for visualization, the turbidity data, water coverage and an RGB true colour image of the source satellite image.

Turbidity data supplied in Formazine Turbidity Units (FTU) and Water Coverage are coloured using a colour scheme which can be found under the  symbol. Water Coverage products also include a white coloured bright pixel flag for clouds to give the user a better understanding on areas potentially obscured by cloudiness. This flag is only valid for products derived from optical sensors as it is obsolete for radar derived products.

To keep the frontend quickly understandable and intuitive, the information load is reduced to a minimum. From a responder perspective it was found important to get a quick visual impression on onsite conditions. Therefore, the data is not displayed sensor-wise and only one product suite can be specified for one of the three datasets. If necessary, the sensor can be implied from the date of the image and the RGB image, which is also supplied for SAR products from Sentinel-1.

Fast responsiveness and information flow are promoted through minimal time taken from user query and visualization on screen. The data is already stored in the GeoServer infrastructure, which allows for fast display even with mediocre internet connection being helpful for first responders out on field operation.

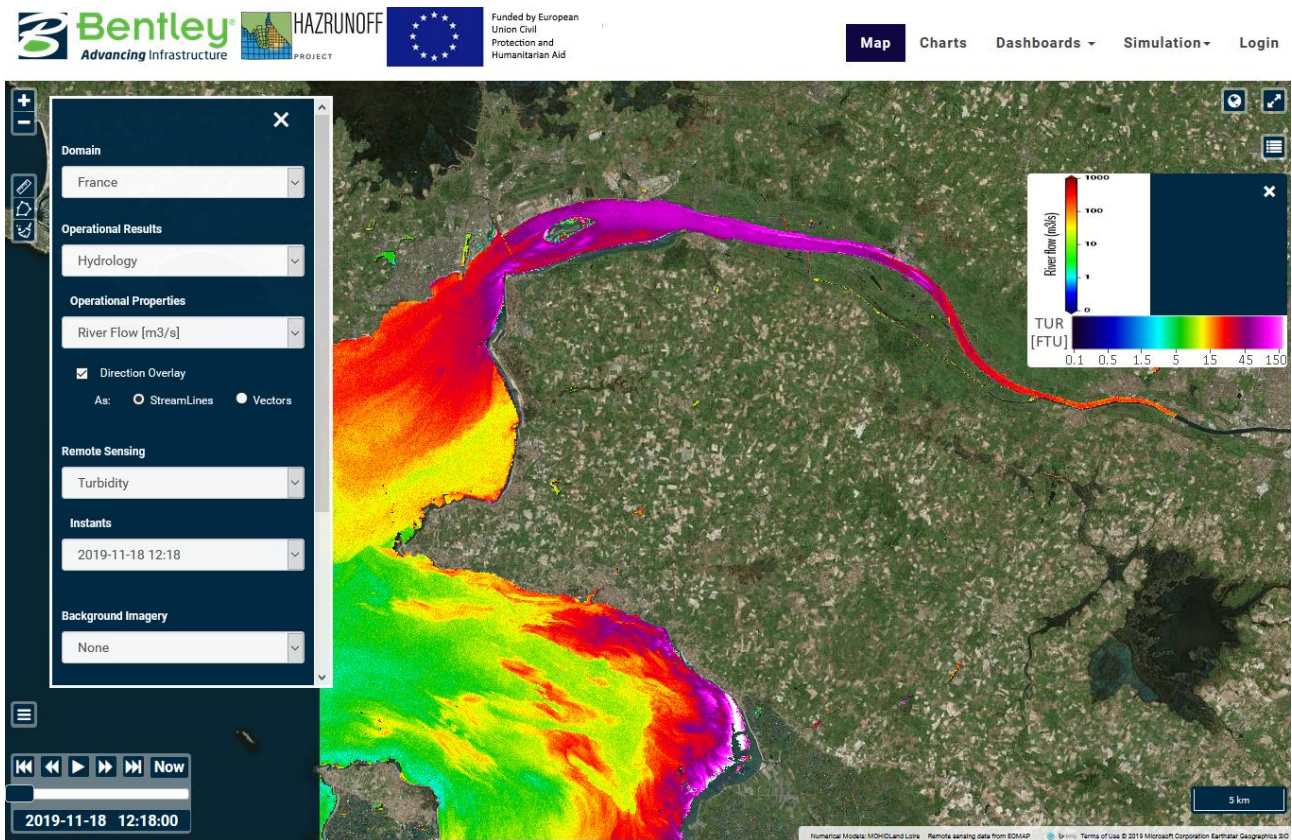


Figure 27: Overview on the HazRunOff WMS interface. Turbidity data (FTU) from Loire estuary.

Model validation for hazards in transitional water

Suspended particulate matter (SPM) causes most of the scattering in natural waters and thus has a strong influence on the underwater light field, and consequently on the whole ecosystem. Turbidity is related to the concentration of SPM which usually is measured gravimetrically, a rather time-consuming method. Measuring turbidity is quick and easy, and therefore also more cost-effective. When derived from remote sensing data the method becomes even more cost-effective due to the good spatial resolution of satellite data and the synoptic capability of the method. Both SPM concentration and turbidity are important parameters describing the water quality of natural waters, and remote sensing retrieved data can provide an efficient method to monitor both. Turbidity is listed as one of the mandatory physical and chemical parameters to be measured within

Annex III of the European Union's Marine Strategy Framework Directive (European Commission 2008, Annex III) for the initial assessment and determination of good environmental status of every marine region or sub-region, especially in coastal zone.

Seasonal changes in precipitation and river discharge alter the SPM concentrations, as increased precipitation leads to increased transport of SPM loads from land to the sea. Increased SPM load can also be caused by hydrodynamic activities, such as upwelling events, by erosion, and by anthropogenic causes, such as dredging. Hence, SPM concentration and turbidity are important factors for understanding these processes within the coastal zone. For detecting SPM changes, long term and high frequency observations are typically required, and the rapid availability of measurements is important for monitoring or detecting current events e.g. during dredging or offshore construction operations. Optical remote sensing satellites has been used for monitoring water turbidity in the coastal zone, in rivers and river plumes. Satellite derived turbidity products are of importance to modelling communities, in terms of validation of and assimilation into sediment transport modelling and assessing dredging operations.

Turbidity data produced as part of WP1 serves the modelling done by IST in WP2, with a focus on the sediment transport modelling component. Water coverage served as validation source for the MOHID Water derived simulations on floods and storm surge. To further calibrate their 3-dimensional models in the Tagus estuary, an SDB has been provided for the coastal area. This model has a spatial resolution of 10m and is thus significantly higher than other publicly available bathymetry datasets.

Conclusions and Recommendations

Throughout the HazRunOff project, EOMAP has implemented its water quality monitoring system for the integration of remote sensing and modelling for early warning and model validation for hazards in transitional water. In four pilot case study sites along the European Atlantic coastline, the operational delivery of the main parameters turbidity and water extent has been set up to provide up-to-date information to the users. The data is made available on a dedicated webtool via standardized interfaces with the data ingested directly after the fully automated processing of the satellite images has produced its quality-controlled outputs. This

almost near-real-time information source enables a quick reaction time of the users in times of e.g. flood events or high sediment loads after heavy rainfall periods. The next step is the introduction of sustainable pricing models to ensure the continuation of the service.

Oil spill identification based on both, SAR imagery and optical data is another product line established during the project. Showcased at major events like the Corsica oil spill in 2018, the workflow has been successfully applied. Still, a set of open research questions need to be addressed during upcoming activities, such as the estimation of oil thickness. For this and in addition for chemical spills, the application of hyperspectral data from sensors like PRISMA and EnMAP is expected to deliver further valuable information in the future.

Appendix

SPILL OCCURENCES PROVIDED BY PHE

Media Source	Year	Type	Setting	Location	Latitude	Longitude	Scale*	Pollutant Type	Key Chemicals	Impact / Effect	Key Words / Terms
https://www.bbc.co.uk/news/uk-england-21350625	2013	Marine Spill	Beach	Devon	50.8	-4.65	VL	Chemical	Polyisobutylene	Environment	chemical gum / dead birds
https://www.bbc.co.uk/news/uk-wales-north-west-wales-43292691	2018	Storm damage	Marina	Holyhead	53.32	-4.64	L	Chemical	Oil and Polystyrene	Environment	Pollution / beach / polystyrene
https://www.bbc.co.uk/news/uk-wales-north-west-wales-38190998	2016	Ship Fire	Port	Liverpool	53.45	-3.01	L	Chemical	VOC	Health	odour / fumes / ship fire
https://www.walesonline.co.uk/news/wales-news/strange-substance-washing-up-welsh-12461785	2017	Beaching of palm oil	Beach	Pembroke	51.6	-4.78	M	Chemical	Palm Oil	Environment	Pollution / wax / beaches
https://www.bbc.co.uk/news/uk-wales-mid-wales-43620665	2018	Slurry leak onto beach	Beach	Ceredigion	52.14	-4.49	M	Slurry	Ammonia / Bio	Health	Discolouration / pollution
https://www.independent.co.uk/news/uk/home-news/noxious-smell-burning-plastic-east-sussex-seaford-a8024161.html https://www.bbc.co.uk/news/uk-england-sussex-42993729	2017	Unknown vapour haze over beaches	Beach	Sussex	50.72	0.22	L	Chemical	VOC	Health	odour / haze / illness
https://www.bbc.co.uk/news/uk-wales-south-east-wales-35157130	2015	Fire in dock	Port	Newport	51.55	-2.98	M	Smoke	VOC	Health	Docks / fire / smoke / smell
https://www.walesonline.co.uk/news/wales-news/river-polluted-after-450000-litres-12845842	2017	Slurry leak into river	River	Monnow	51.9	-3	L	Slurry	Ammonia / Bio	Environment	Fish Kill / River pollution

https://www.bbc.co.uk/news/uk-wales-south-west-wales-39869759	2016	Oil Pipeline Leak inland	River	Carmarthen	51.8	-4.25	VL	Oil	Kerosene	Environment / Health	Fish Kill / River pollution
---	------	--------------------------	-------	------------	------	-------	----	-----	----------	----------------------	-----------------------------